A SIMPLE ELASTOPLASTIC MODEL FOR NORMALLY AND OVER CONSOLIDATED SOILS WITH UNIFIED MATERIAL PARAMETERS

Teruo Nakai[i] and Masaya Hinokio[ii]

ABSTRACT

An isotropic hardening elastoplastic model for soil, which can describe typical deformation and strength behavior of normally and over-consolidated soils in general stress conditions, is presented. This model can take into consideration the influence of density and/or confining pressure on the deformation and strength characteristics of soils. Further, it also takes into account the influence of intermediate principal stress on the deformation and strength of soil and the stress path dependency on the plastic flow, as did other previous versions of this model. For considering the intermediate principal stress on the deformation and strength, the concept of modified stress t_{ij} is employed in the same way as the previous models. With respect to the subloading surface concept, the previous models are revised and extended into one in which the influence of density and/or confining pressure on the deformation and strength of soil can be considered. Furthermore, the influence of stress path dependency of the direction of plastic flow is considered by dividing the plastic strain increment into two components – i.e., a component satisfying associated flow rule and a component of isotropic compression. In the present model, only one material parameter a for representing the influence of density and/or confining pressure is added to the parameters of the previous model, which are fundamentally the same as those of the Cam clay model. The validity of the present model is checked by monotonic and cyclic loading tests not only on normally and over-consolidated clay but also on loose and dense sands in three-dimensional stresses.

Key words: clay, (confining pressure), constitutive equation of soil, deformation, density, (intermediate principal stress), plasticity, sand, strength, (stress path dependency) (IGC: D6)

INTRODUCTION

For appropriate prediction of the deformation and failure of soil, we have to carry out numerical analysis using a simple and generalized constitutive model for soils. The Cam clay model, which was developed at Cambridge University (e.g., Schofield and Wroth, 1968), was the first elastoplastic model applicable to the practical deformation analysis of ground. This model is certainly very simple, i.e., the number of material parameters is few, and the meaning of each parameter is clear. However, the Cam clay model encounters problems for description of soil behavior in the following points:

(i)   Influence of intermediate principal stress on the deformation and strength of soil
(ii) Stress path dependency on the direction of plastic flow
(iii) Positive dilatancy during strain hardening
(iv) Soil anisotropy and non-coaxiality
(v)   Behavior of soil under cyclic loading
(vi) Influence of density and/or confining pressure on the deformation and strength
(vii) Behavior of structured soil
(viii) Time effect and age effect

Although many models have been proposed since the Cam clay model, most of them are much more complex than the Cam clay model, and their applicability to practical problems is still limited. We also have developed simple constitutive models for clay and sand - named t_{ij}-clay model (Nakai and Matsuoka, 1986) and t_{ij}-sand model (Nakai, 1989) – and applied them to the analysis of practical geotechnical problems. In these models, the influence of intermediate principal stress on the deformation and strength of soil and the stress path dependency of plastic flow are particularly taken into consideration. However, the t_{ij}-clay model is applicable to normally consolidated clays but cannot describe the elastoplastic behavior of over consolidated clays with positive dilatancy, and some material parameters of the t_{ij}-sand model depend on the density and/or confining pressure even for the same sand. On the other hand, even when the clayey ground is initially normally consolidated, the ground condition can change to over-consolidated during loading

[i] Professor of Geotechnical Engineering, Department of Civil Engineering, Nagoya Institute of Technology, Gokiso-cho, Showa-ku, Nagoya 466-8555, Japan (nakai@tutil.ace.nitech.ac.jp).
[ii] Research Associate, ditto.

and unloading processes. The void ratio of sandy ground also can change during deformation. Then, in order to predict the ground movements and its failure behavior precisely, it is necessary that the model used in the analysis be capable of describing the deformation and strength accurately under a wide range of soil density and/or confining pressure with unified material parameters.

In the present study, the above models for clay and sand are extended to a simple model that can take into account the influence of the density and/or confining pressure on the deformation and strength of soil, as well as the influence of intermediate principal stress on the deformation and strength and the influence of the stress path on the plastic flow. After describing the concept of t_{ij} and the outline of the Cam clay model, we will show the formulation of the present model and its validation by experimental results.

EXPLANATION OF T_{ij}-CONCEPT AND OUTLINE OF CAM CLAY MODEL

Concept of t_{ij}

In most isotropic hardening models such as the Cam clay model, yield functions are formulated using stress parameters (mean stress p and deviator stress q) and assuming flow rule in ordinary stress space σ_{ij}. However, such models cannot describe stress-strain behavior and strength in three-dimensional stresses in a uniform manner. Figure 1 shows the results of drained triaxial compression and extension tests on Fujinomori clay under constant mean principal stress, in terms of the relation between stress ratio (q/p), deviatoric strain (ε_d) and volumetric strain (ε_v). It can be seen from this figure that the deformation and strength characteristics of soils cannot be explained adequately using these stress and strain parameters. Nakai and Mihara (1984), then, proposed a method, which has been called the t_{ij}-concept, to take into account adequately the influence of intermediate principal stress on soil behavior, by introducing the modified stress tensor t_{ij} and assuming the flow rule in a modified stress space. The stress and strain increment tensors and their parameters using the ordinary concept and t_{ij}-concept are compared in Table 1. As shown in Fig. 2, the stress tensors and parameters in the ordinary

models are defined as the quantities related to normal and parallel components of σ_{ij} to the octahedral plane. On the other hand, as shown in Fig. 3, the stress tensors and stress parameters of the t_{ij}-concept are those of normal and parallel components of the modified stress t_{ij} to the spatially mobilized plane (briefly SMP; Matsuoka and Nakai, 1974). Here, a_{ij} is the symmetric tensor whose principal values are determined by the direction cosines (a_1, a_2 and a_3) of the normal to the SMP. The tensor a_{ij}
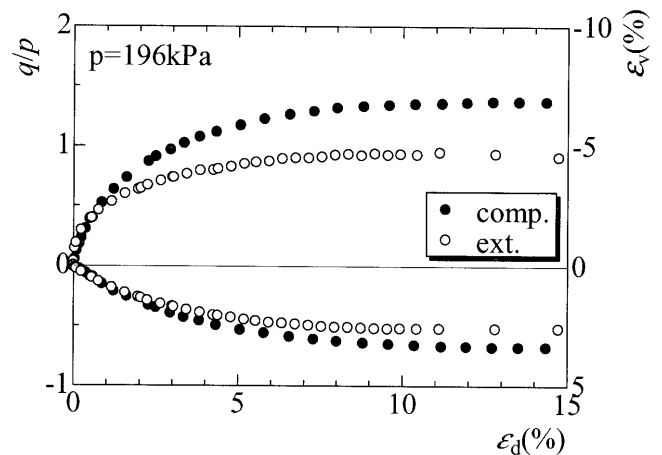

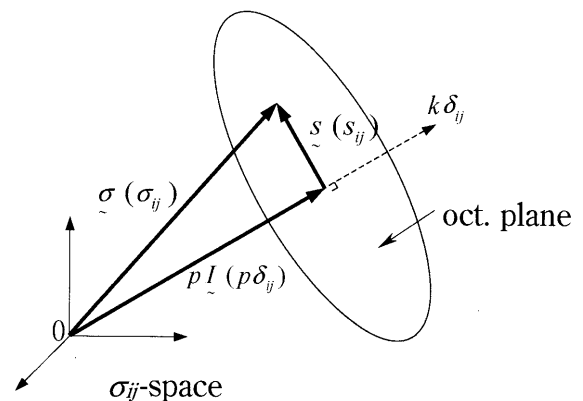Fig. 1.   Test results of triaxial compression and extension tests

Fig. 2.   Illustration of stress quantities in σ_{ij}-space which are used in the ordinary concept

Table 1.   Comparison of tensors and scalars related to stress and strain increment between ordinary concept and t_{ij}-concept

|	Ordinary concept	t_{ij} concept
Tensor normal to reference plane	δ_{ij} (unit tensor)	a_{ij} (tensor normal to SMP)
Stress tensor	σ_{ij}	$t_{ij} = a_{ik}\sigma_{kj}$
Mean stress	$p = \sigma_{ij}\delta_{ij}/3$	$t_N = t_{ij}a_{ij}$
Deviatoric stress tensor	$s_{ij} = \sigma_{ij} - p\delta_{ij}$	$t'_{ij} = t_{ij} - t_N a_{ij}$
Deviatoric stress	$q = \sqrt{(3/2)s_{ij}s_{ij}}$	$t_S = \sqrt{t'_{ij}t'_{ij}}$
Stress ratio tensor	$\eta_{ij} = s_{ij}/p$	$x_{ij} = t'_{ij}/t_N$
Stress ratio	$\eta \equiv q/p = \sqrt{(3/2)\eta_{ij}\eta_{ij}}$	$X \equiv t_S/t_N = \sqrt{x_{ij}x_{ij}}$
Strain increment normal to reference plane	$d\varepsilon_v = d\varepsilon_{ij}\delta_{ij}$	$d\varepsilon^*_{SMP} = d\varepsilon_{ij}a_{ij}$
Deviatoric strain increment tensor	$de_{ij} = d\varepsilon_{ij} - d\varepsilon_v\delta_{ij}/3$	$d\varepsilon'_{ij} = d\varepsilon_{ij} - d\varepsilon^*_{SMP}a_{ij}$
Strain increment parallel to reference plane	$d\varepsilon_d = \sqrt{(2/3)de_{ij}de_{ij}}$	$d\gamma^*_{SMP} = \sqrt{d\varepsilon'_{ij}d\varepsilon'_{ij}}$
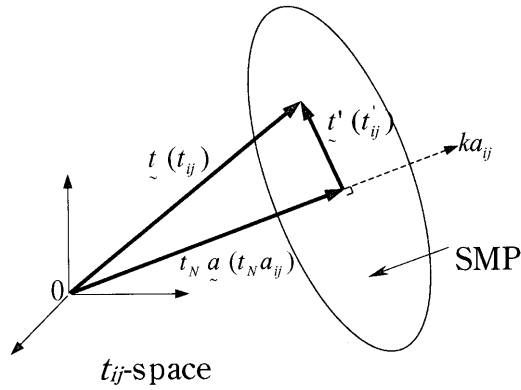
t_{ij}-space

Fig. 3. Illustration of stress quantities in t_{ij}-space which are used in the t_{ij} concept

Fig. 4. Yield surface of Cam clay model on p-q plane

and its principal values are expressed as follows using σ_{ij} (Nakai, 1989):

$$a_{ij}=\sqrt{\frac{I_3}{I_2}}\cdot r_{ij}^{-1}=\sqrt{\frac{I_3}{I_2}}\cdot(\sigma_{ik}+I_{r2}\delta_{ik})(I_{r1}\sigma_{kj}+I_{r3}\delta_{kj})^{-1} \quad (1)$$

$$a_i=\sqrt{\frac{I_3}{I_2\sigma_i}} \quad (i=1, 2, 3) \quad (2)$$

where σ_i ($i=1, 2, 3$) are the three principal stresses, I_1, I_2, and I_3 are the first, second and third invariants of σ_{ij}, and I_{r1}, I_{r2} and I_{r3} are the first, second and third invariants of r_{ij}, which is the stress tensor to the one-half power, such that $r_{ik}r_{kj}=\sigma_{ij}$. These invariants are expressed using principal stresses and stress tensors as

$$\left.\begin{array}{l} I_1=\sigma_1+\sigma_2+\sigma_3=\sigma_{ii} \\[2mm] I_2=\sigma_1\sigma_2+\sigma_2\sigma_3+\sigma_3\sigma_1=\dfrac{1}{2}\{(\sigma_{ii})^2-\sigma_{ij}\sigma_{ji}\} \\[2mm] I_3=\sigma_1\sigma_2\sigma_3=e_{ijk}\sigma_{i1}\sigma_{j2}\sigma_{k3} \end{array}\right\} \quad (3)$$

$$\left.\begin{array}{l} I_{r1}=\sqrt{\sigma_1}+\sqrt{\sigma_2}+\sqrt{\sigma_3}=r_{ii} \\[2mm] I_{r2}=\sqrt{\sigma_1\sigma_2}+\sqrt{\sigma_2\sigma_3}+\sqrt{\sigma_3\sigma_1}=\dfrac{1}{2}\{(r_{ii})^2-r_{ij}r_{ji}\} \\[2mm] I_{r3}=\sqrt{\sigma_1\sigma_2\sigma_3}=e_{ijk}r_{i1}r_{j2}r_{k3} \end{array}\right\} \quad (4)$$

where e_{ijk} is the permutation symbol. As can be seen from the above equation, a_{ij} is a function of the stress ratio and its principal axes coincide with those of σ_{ij} (the methods to calculate a_{ij} in plane strain, axisymmetric and general 3D conditions are shown in **Appendix I**). The modified stress tensor is then defined by the product of a_{ik} and σ_{kj} as follows:

$$t_{ij}=a_{ik}\sigma_{kj} \quad (5)$$

The principal axes of t_{ij} coincide with those of σ_{ij}, because the principal axes of a_{ij} and σ_{ij} are identical.

In the isotropic hardening model based on the t_{ij}-concept, we formulated the yield function using the stress parameters (t_N and t_S) instead of (p and q) and assumed the flow rule not in σ_{ij} space but in t_{ij} space. The validity of this concept was confirmed by the test results on clay
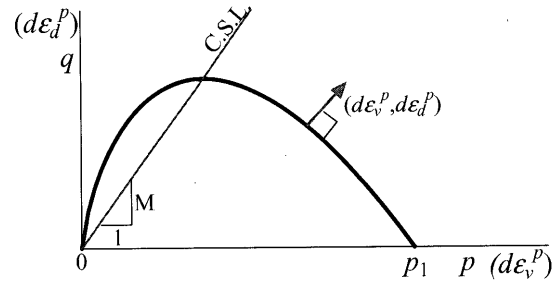
(Nakai and Mastuoka, 1986; Nakai, et al., 1986) and sand (Nakai, 1989) in general stress conditions.

Brief Description of Cam Clay Model

The yield function of the Cam clay model (e.g., Schofield and Wroth, 1968), which is the same as the plastic potential function, is represented in Fig. 4, and it is given by a function of mean principal stress p and stress ratio η.

$$f=\ln p+\frac{\eta}{M}-\ln p_1=0 \quad (6)$$

Here, M is the stress ratio at critical state η_{CS} and is represented by using the principal stress ratio at critical state in triaxial compression $R_{CS}\equiv(\sigma_1/\sigma_3)_{CS(comp.)}$ as

$$M=\frac{3(R_{CS}-1)}{R_{CS}+2} \quad (7)$$

In Eq. (6), p_1 is related to the strain hardening parameter (plastic volumetric strain ε_v^p) as follows:

$$\varepsilon_v^p=C_p\ln\frac{p_1}{p_0} \quad \left(C_p=\frac{\lambda-\kappa}{1+e_0}\right) \quad (8)$$

where p_0 is the value of the initial yield surface at p-axis, and p_1 is that of the current yield surface. The symbols e, λ and κ denote void ratio, compression index and swelling index, respectively, and e_0 is the void ratio at reference state. The flow rule and the proportionality constant are represented as

$$d\varepsilon_{ij}^p=\Lambda\frac{\partial f}{\partial\sigma_{ij}} \quad (9)$$

$$\Lambda=\frac{df_\sigma}{h^p}=\frac{\dfrac{\partial f}{\partial\sigma_{ij}}d\sigma_{ij}}{h^p}=\frac{\dfrac{\partial f}{\partial\sigma_{ij}}d\sigma_{ij}}{\dfrac{1}{C_p}\dfrac{\partial f}{\partial\sigma_{kk}}} \quad (10)$$

The loading condition is expressed as follows:

$$\begin{cases} d\varepsilon_{ij}^p\neq 0 & \text{if } f=0 \text{ and } df_\sigma=\dfrac{\partial f}{\partial\sigma_{ij}}d\sigma_{ij}>0 \\[3mm] d\varepsilon_{ij}^p=0 & \text{else} \end{cases} \quad (11)$$

Now, the coaxiality between stresses and plastic strain increments and normality condition give the following equation between the stress parameters and the plastic strain increment parameters:
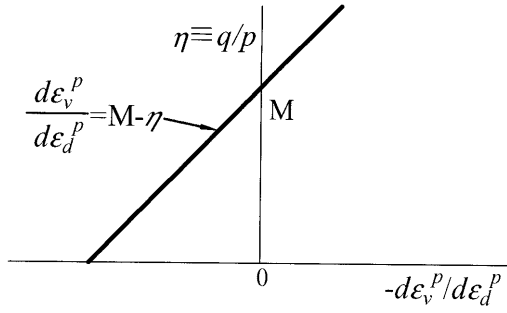
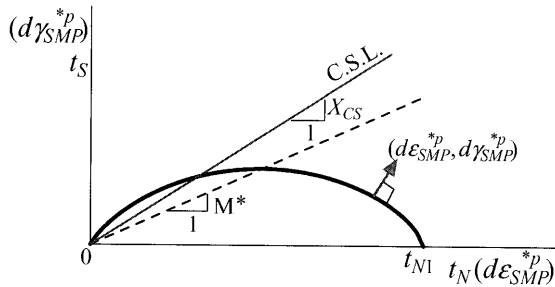Fig. 5.   Stress ratio-plastic strain increment ratio relation of Cam clay model
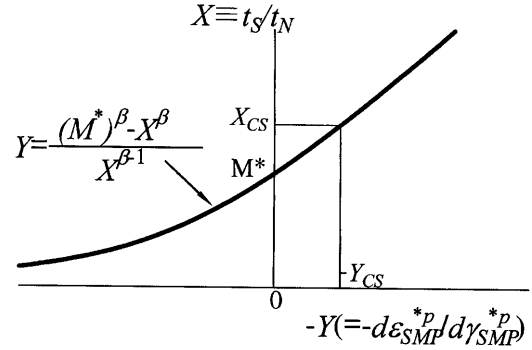

Fig. 7.   Stress ratio-plastic strain increment ratio relation of the proposed model

$$M^* = (X_{CS}^\beta + X_{CS}^{\beta-1} Y_{CS})^{1/\beta} \tag{16}$$

and these ratios X_{CS} and Y_{CS} are represented by the principal stress ratio at critical state in triaxial compression R_{CS} (see **Appendix II** for the detailed derivation process of Eqs. (16), (17) and (18)):

$$X_{CS} = \frac{\sqrt{2}}{3} \left(\sqrt{R_{CS}} - \frac{1}{\sqrt{R_{CS}}} \right) \tag{17}$$

$$Y_{CS} = \frac{1 - \sqrt{R_{CS}}}{\sqrt{2}(\sqrt{R_{CS}} + 0.5)} \tag{18}$$

From the normality condition, the following relation holds between the stress parameters and the plastic strain increment parameters based on the t_{ij}-concept.

$$t_N \cdot d\varepsilon_{SMP}^{*p} + t_S \cdot d\gamma_{SMP}^{*p} = 0 \tag{19}$$

Here, the directions of $d\varepsilon_{SMP}^{*p}$ and $d\gamma_{SMP}^{*p}$ coincide with those of t_N and t_S, respectively, because coaxialty between stress and plastic strain increment are assumed. The stress ratio-plastic strain increment ratio relation in the following equation (see Fig. 7) is obtained from Eqs. (14), (15) and (19).

$$Y = \frac{(M^*)^\beta - X^\beta}{X^{\beta-1}} \tag{20}$$

The difference of shape of the yield surfaces between the present model and the previous models (Nakai and Matsuoka, 1986; Nakai, 1989), and the merits of the present model are described by Chowdhury and Nakai (1998). In the previous models, we assumed a liner relation between the stress ratio and plastic strain increment ratio so that their yield surfaces have singular points at the origin and t_N-axis. In contrast, the present model has no singular point on the yield surface. The plastic strain increment can be calculated by assuming the associated flow rule in t_{ij} space.

$$d\varepsilon_{ij}^p = \Lambda \frac{\partial f}{\partial t_{ij}} \tag{21}$$

Here, Λ is the proportionality constant which represents the magnitude of the plastic strain increment in the same way as in ordinary elastoplastic models.

Now, for the previous model for normally consolidated clay (t_{ij}-clay model), t_{N1} in Eq. (14) is linked with

Fig. 6.   Yield surface of proposed model on t_N-t_S plane

$$p \cdot d\varepsilon_v^p + q \cdot d\varepsilon_d^p = 0 \tag{12}$$

Then, the plastic strain increments whose direction is normal to the yield function in Eq. (6) satisfy the following stress ratio-plastic strain increment ratio relation (see Fig. 5):

$$\frac{d\varepsilon_v^p}{d\varepsilon_d^p} = M - \eta \tag{13}$$

FORMULATION OF SUBLOADING T_{ij} MODEL

Model Satisfying Associated Flow Rule in t_{ij} Space

Usually, the yield function of soil is presented as a logarithmic function of the mean stress plus an increasing function of stress ratio. Using the stress parameters of t_{ij}-concept in Table 1, we give the yield function in the following form:

$$f = \ln t_N + \varsigma(X) - \ln t_{N1}$$

$$= \ln \frac{t_N}{t_{N0}} + \varsigma(X) - \ln \frac{t_{N1}}{t_{N0}} = 0 \tag{14}$$

$$\varsigma(X) = \frac{1}{\beta} \left(\frac{X}{M^*} \right)^\beta \quad (\beta: \text{material parameter}) \tag{15}$$

Here, t_N and $X \equiv t_S/t_N$ are the mean stress and the stress ratio based on the t_{ij}-concept, and t_{N1} determines the size of the yield surface (the value of t_N at $X=0$). Figure 6 shows a two-dimensional representation of the yield surface on the $t_N - t_S$ plane. The value of M^* in Eq. (15) is expressed as follows using principal stress ratio $X_{CS} \equiv (t_S/t_N)_{CS}$ and plastic strain increment ratio $Y_{CS} \equiv (d\varepsilon_{SMP}^{*p}/d\gamma_{SMP}^{*p})_{CS}$ at critical state:

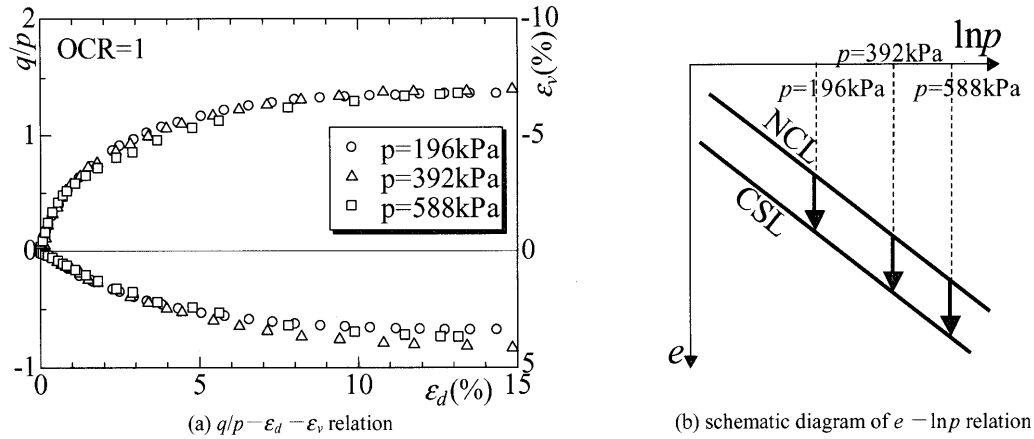(a) $q/p-\varepsilon_d-\varepsilon_v$ relation

(b) schematic diagram of $e-\ln p$ relation

Fig. 8. Test results of triaxial compression tests on normally consolidated clay (OCR = 1) under constant mean principal stress

(a) $q/p-\varepsilon_d-\varepsilon_v$ relation
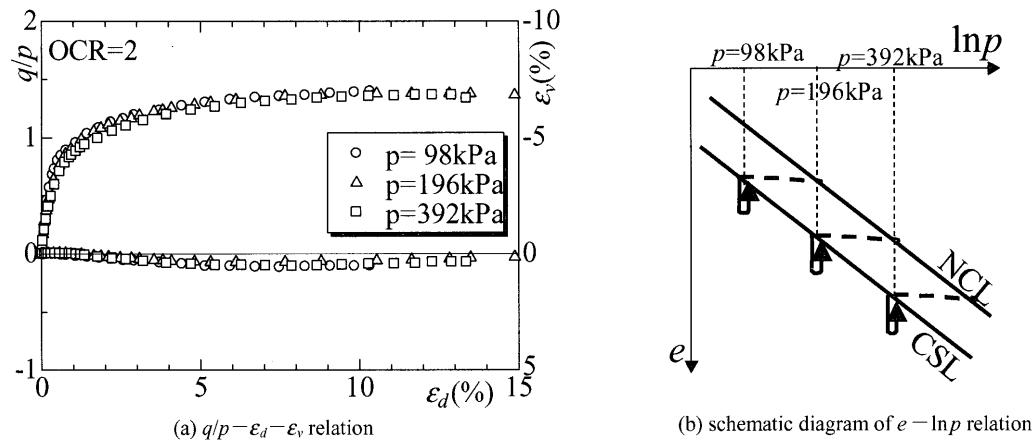
(b) schematic diagram of $e-\ln p$ relation

Fig. 9. Test results of triaxial compression tests on over-consolidated clay (OCR = 2) under constant mean principal stress

the plastic volumetric strain ε_v^p as indicated by Eq. (8) in the same manner as in the Cam clay model.

$$\varepsilon_v^p = C_p \ln \frac{t_{N1}}{t_{N0}} \quad \left(C_p = \frac{\lambda - \kappa}{1 + e_0}\right) \tag{22}$$

This equation is obtained from the condition that the plastic volumetric strain (or void ratio) of normally consolidated clay at elastoplastic region is determined by the present stress state alone and is independent of the stress path history (Henkel, 1960), and the mean stress t_N based on t_{ij}-concept coincides with the ordinary mean principal stress p at isotropic stress condition ($X=0$). Here, e_0 is the void ratio at reference state ($X=0$ and $p=t_N=t_{N0}$). Then, from Eqs. (14), (21) and (22) and compatibility condition ($df=0$), we obtain the following equation:

$$df = \frac{\partial f}{\partial \sigma_{ij}} d\sigma_{ij} - \frac{1}{C_p} d\varepsilon_v^p$$

$$= \frac{\partial f}{\partial \sigma_{ij}} d\sigma_{ij} - \frac{1}{C_p} \Lambda \frac{\partial f}{\partial t_{hh}} = 0 \tag{23}$$

Then, the proportionality constant Λ is expressed as follows in the same way as the previous model (Nakai and Matsuoka, 1986):

$$\Lambda = \frac{df_\sigma}{h^p} = \frac{\dfrac{\partial f}{\partial \sigma_{ij}} d\sigma_{ij}}{h^p} = \frac{\dfrac{\partial f}{\partial \sigma_{ij}} d\sigma_{ij}}{\dfrac{1}{C_p} \dfrac{\partial f}{\partial t_{kk}}} \tag{24}$$

where, denominator h^p is the plastic modulus that represents the stiffness of plastic components.

On the other hand, an over-consolidated clay does not satisfy Eq. (22), and its stiffness is larger (h^p of over-consolidated clays is larger than that in Eq. (24)). Figures 8 to 10 show (a) observed relations between stress ratio q/p, deviatoric strain ε_d and volumetric strain ε_v of triaxial compression tests on Fujinomori clay under various over-consolidation ratios (OCR = 1, 2 and 4) and various mean principal stresses, and (b) schematic changes of void ratio in these tests on e-$\ln p$ plane. Here, the straight lines NCL and CSL in diagram (b) are the normally consolidation line ($X=0$) and critical state line ($X=X_{CS}$). We can see from these figures that the stiffness of stress ratio against strains increases with an increase of the over-consolidation ratio but is independent of mean stresses. Taking into consideration the above test results and referring to the subloading surface concept proposed by Hashiguchi and Ueno (1977) and Hashiguchi (1980), we will extend the previous model to one applicable to not
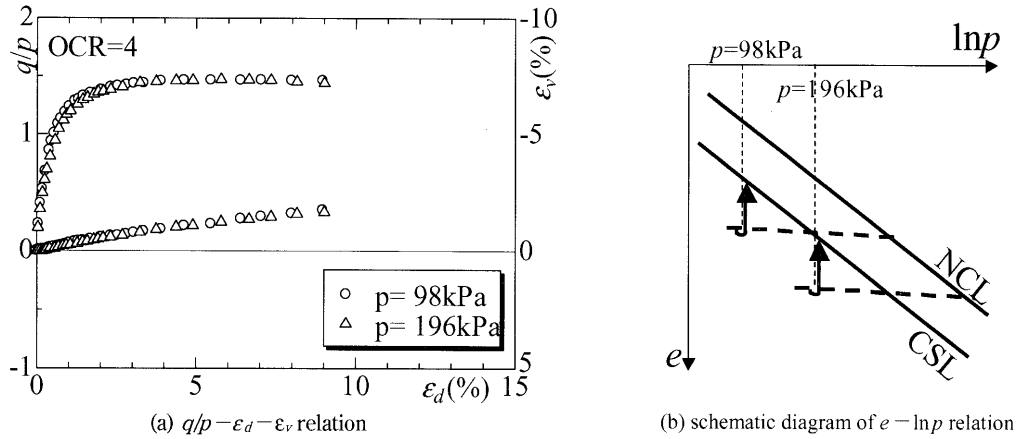
(a) $q/p - \varepsilon_d - \varepsilon_v$ relation

(b) schematic diagram of $e - \ln p$ relation

Fig. 10. Test results of triaxial compression tests on over-consolidated clay (OCR = 4) under constant mean principal stress
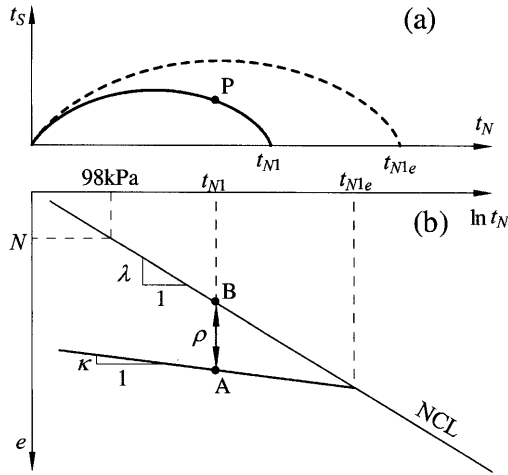

Fig. 11. Shape of yield surface and normal yield surface, and definition of ρ

only normally consolidated soils but also to over-consolidated soils. According to the subloading surface concept, the yield surface (subloading surface) not only has to expand but also to shrink for the present stress state to lie always on the surface, and the yield function represented by Eq. (14) is rewritten as

$$f = \ln \frac{t_N}{t_{N0}} + \varsigma(X) - \ln \frac{t_{N1}}{t_{N0}}$$

$$= \ln \frac{t_N}{t_{N0}} + \varsigma(X) - \left(\ln \frac{t_{N1e}}{t_{N0}} - \ln \frac{t_{N1e}}{t_{N1}} \right) = 0 \qquad (25)$$

Here, t_{N1} is the value of t_N of the yield surface passing through the present stress state in the same manner as Fig. 6, and t_{N1e} is the mean stress t_N equivalent to the present plastic volumetric strain (or void ratio), which is defined as

$$\varepsilon_v^p = C_p \ln \frac{t_{N1e}}{t_{N0}} \qquad \left(C_p = \frac{\lambda - \kappa}{1 + e_0} \right) \qquad (26)$$

Although t_{N1e} coincides with t_{N1} in normally consolidated states, t_{N1e} is larger than t_{N1} in over-consolidated states. The ratio t_{N1e}/t_{N1} corresponds to the over-consolidation ratio in a broad sense. Figure 11(a) shows the yield sur-

face (solid curve) passing through the present stress state P and its similar curve passing through t_{N1e} on t_N axis, which is the yield surface for a normally consolidated soil with same void ratio (broken curve). In the subloading concept by Hashiguchi (1980), the solid curve and broken curve are called subloading surface and normal yield surface, respectively. Assuming a rational evolution rule for the size of both curves with plastic strain developments, Hashiguchi (1980) proposed a method to describe unconventional plasticity behavior as seen in over-consolidated clay. Introducing this concept directly, Asaoka et al. (1997) extended the Cam clay model to one valid for over-consolidated clay as well. The previous t_{ij}-clay model was also extended using the subloading concept and others by Chowdhury et al. (1999). In the present study, we intend to revise the concept, while preserving the basic idea of Hashiguchi, to make it more suitable for observed soil behavior and easier to apply. Now, the points A and B on the e-$\ln t_N$ diagram in Fig. 11(b) indicate the void ratios of over-consolidated soil and normally consolidated soil at the same stress state P. The difference of the void ratios ρ between A and B can be regarded as an index of soil density, because the stress ratio-strains relations of soils with the same ρ are identical regardless of mean stress (see Figs. 8 to 10). In a mechanical sense, void ratio itself is, therefore, not suitable for representing the soil density. We can see from Fig. 11 that there is the following relation between ρ and the ratio t_{N1e}/t_{N1}.

$$\rho = (\lambda - \kappa) \ln \frac{t_{N1e}}{t_{N1}} = (1 + e_0) C_p \ln \frac{t_{N1e}}{t_{N1}} \qquad (27)$$

From Eqs. (25) to (27), we can obtain

$$f = \ln \frac{t_N}{t_{N0}} + \varsigma(X) - \frac{1}{C_p} \left(\varepsilon_v^p - \frac{\rho}{1 + e_0} \right) \qquad (28)$$

Compatibility condition ($df = 0$) gives

$$df = \frac{\partial f}{\partial \sigma_{ij}} d\sigma_{ij} - \frac{1}{C_p} \left(d\varepsilon_v^p - d \left(\frac{\rho}{1 + e_0} \right) \right)$$

$$= \frac{\partial f}{\partial \sigma_{ij}} d\sigma_{ij} - \frac{1}{C_p} \left(\Lambda \frac{\partial f}{\partial t_{ii}} - d \left(\frac{\rho}{1 + e_0} \right) \right) = 0 \qquad (29)$$

Here, we assume that the increment of $\rho/(1+e_0)$, which represents the change of density during plastic deformation, is influenced by the present density ρ and mean stress t_N. Then, it can be given by the following equation using a function $L(\rho, t_N)$.

$$d\left(\frac{\rho}{1+e_0}\right) = \Lambda \cdot L(\rho, t_N) \tag{30}$$

Therefore, from Eqs. (29) and (30), the proportionality constant Λ for an over-consolidated soil is expressed as

$$\Lambda = \frac{df_\sigma}{h^p} = \frac{\dfrac{\partial f}{\partial \sigma_{ij}} d\sigma_{ij}}{h^p} = \frac{\dfrac{\partial f}{\partial \sigma_{ij}} d\sigma_{ij}}{\dfrac{1}{C_p}\left(\dfrac{\partial f}{\partial t_{kk}} - L(\rho, t_N)\right)} \tag{31}$$

Here, $L(\rho, t_N)$ has to be formulated to explain the behavior from a normally consolidated condition to an over-consolidation state: i.e., (i) whenever plastic deformation occurs, Λ is positive; (ii) the over-consolidated state moves toward the normally consolidated state with development of plastic deformation, so that the increment $d(\rho/(1+e_0))$ should be negative; (iii) Eq. (31) becomes Eq. (24) at normally consolidated state ($\rho = 0$). To satisfy these conditions, the function $L(\rho, t_N)$ should be negative at $\rho > 0$ and $L(\rho, t_N) = 0$ at $\rho = 0$. Now, we will pay attention to the unique relation between stress ratio and strains regardless of mean principal stresses in Figs. 8 to 10. The plastic strain increments for normally consolidated soil calculated using Eq. (24) satisfy the unique relation in Fig. 8 in the same way as the Cam clay model. In order to describe the unique relations (Figs. 9 and 10) in over-consolidated states as well, the dimension of $L(\rho, t_N)$ in Eq. (31) has to be the same as $\partial f/\partial t_{ii}$. Furthermore, the stiffness and strength of over-consolidated soils become large with an increase of density ρ. Here, the denominator of h^p in Eq. (31) represents the stiffness, and the relation between density and peak strength is obtained from the condition of $h^p = 0$. Satisfying the above conditions, we define $L(\rho, t_N)$ as

$$L(\rho, t_N) = -\frac{G(\rho)}{t_N} \tag{32}$$

and Eq. (31) is rewritten as

$$\Lambda = \frac{df_\sigma}{h^p} = \frac{\dfrac{\partial f}{\partial \sigma_{ij}} d\sigma_{ij}}{h^p} = \frac{\dfrac{\partial f}{\partial \sigma_{ij}} d\sigma_{ij}}{\dfrac{1}{C_p}\left(\dfrac{\partial f}{\partial t_{kk}} + \dfrac{G(\rho)}{t_N}\right)}$$

$$= \left(\frac{\dfrac{\partial f}{\partial \sigma_{ij}} D^e_{ijkl} d\varepsilon_{kl}}{h^p + \dfrac{\partial f}{\partial \sigma_{mn}} D^e_{mnop} \dfrac{\partial f}{\partial t_{op}}}\right) \tag{33}$$

The derivation process of the proportionality constant Λ expressed by the strain increment $d\varepsilon_{ij}$ and the elastic modulus tensor D^e_{ijkl} is shown in **Appendix III**. Here, $G(\rho)$ is a monotonically increasing function which satisfies the condition of $G(0) = 0$. We will give it by the following

equation using one material parameter a.

$$G(\rho) = a \cdot \rho^2 \tag{34}$$

The loading condition of soil through its hardening process to softening process is presented as follows, in the same way as Hashiguchi (1980), Asaoka et al. (1994, 1997), Chowdhury et al. (1999) and others:

$$\begin{cases} d\varepsilon^p_{ij} \neq 0 & \text{if} \quad \Lambda = \dfrac{df_\sigma}{h^p} \geq 0 \\[2mm] d\varepsilon^p_{ij} = 0 & \text{if} \quad \Lambda = \dfrac{df_\sigma}{h^p} < 0 \end{cases}$$

or

$$\begin{cases} d\varepsilon^p_{ij} \neq 0 & \text{if} \quad \dfrac{\partial f}{\partial \sigma_{ij}} D^e_{ijkl} d\varepsilon_{kl} \geq 0 \\[2mm] d\varepsilon^p_{ij} = 0 & \text{if} \quad \dfrac{\partial f}{\partial \sigma_{ij}} D^e_{ijkl} d\varepsilon_{kl} < 0 \end{cases} \tag{35}$$

The plastic strain increment can be finally written as follows including its loading condition.

$$d\varepsilon^p_{ij} = \langle \Lambda \rangle \frac{\partial f}{\partial t_{ij}} = \left\langle \frac{df_\sigma}{h^p} \right\rangle \frac{\partial f}{\partial t_{ij}} \tag{36}$$

Here, the symbol $\langle \rangle$ denotes the Macaulay bracket, i.e., $\langle A \rangle = A$ if $A \geq 0$; otherwise $\langle A \rangle = 0$.

The elastic strain increment is given by generalized Hooke's law

$$d\varepsilon^p_{ij} = \frac{1+\nu_e}{E_e} d\sigma_{ij} - \frac{\nu_e}{E_e} d\sigma_{kk}\delta_{ij} \tag{37}$$

Young's modulus E_e is expressed in terms of the swelling index κ and Poisson's ratio ν_e as

$$E_e = \frac{3(1-2\nu_e)(1+e_0)p}{\kappa} \tag{38}$$

Therefore, the total strain increment is given by

$$d\varepsilon_{ij} = d\varepsilon^e_{ij} + d\varepsilon^p_{ij} \tag{39}$$

Extension to Model Considering Stress Path Dependency on the Direction of Plastic Flow

According to usual plasticity, the direction of plastic flow (direction of plastic strain increments) is independent of the direction of stress increments. It is, however, experimentally known that the direction of plastic flow is influenced by the direction of stress increments except at and after peak strength. In the previous models for clay and sand (t_{ij}-clay model and t_{ij}-sand model), such stress path dependency was considered by dividing the plastic strain increment into two components – the plastic strain increment $d\varepsilon^{p(AF)}_{ij}$ satisfying the associated flow rule in t_{ij}-space as mentioned above and the isotropic plastic strain increment $d\varepsilon^{p(IC)}_{ij}$ under increasing mean stress – in spite of using just one yield function and one strain hardening parameter. The same method is employed in the present modeling to consider the stress path dependency on the direction of plastic flow. Referring to Eqs. (21) and (33), we can express the plastic volumetric strain increment by

$$d\varepsilon_v^p = d\varepsilon_{ii}^p = \Lambda \frac{\partial f}{\partial t_{ii}} = \frac{df_\sigma}{\frac{1}{C_p}\left(\frac{\partial f}{\partial t_{kk}} + \frac{G(\rho)}{t_N}\right)} \cdot \frac{\partial f}{\partial t_{ii}} \qquad (40)$$

Under isotropic compression condition ($X=0$), the following equations hold.

$$t_{N1} = t_N = p \qquad (41)$$

$$\frac{\partial f}{\partial t_{ii}} = \frac{1}{t_N} a_{ii} \qquad (42)$$

and the plastic volumetric strain increment is expressed as

$$d\varepsilon_v^p = \frac{1}{\frac{1}{C_p}\left(1 + \frac{G(\rho)}{a_{ii}}\right)} \cdot \frac{dt_N}{t_N} \qquad (43)$$

It is assumed that the plastic volumetric isotropic strain increment $d\varepsilon_v^{p(IC)}$ in general stress conditions, which occurs at $dt_N > 0$, is t_N/t_{N1} of the plastic volumetric strain $d\varepsilon_v^p$ given by Eq. (43) in the same way as the t_{ij}-clay model (Nakai and Matsuoka, 1986).

$$d\varepsilon_v^{p(IC)} = \frac{1}{\frac{1}{C_p}\left(1 + \frac{G(\rho)}{a_{ii}}\right)} \cdot \frac{\langle dt_N \rangle}{t_N} \cdot \frac{t_N}{t_{N1}} \qquad (44)$$

where, from Eq. (14), the ratio t_N/t_{N1} is expressed by the following equation:

$$\frac{t_N}{t_{N1}} = \exp\left(-\varsigma(X)\right) = \exp\left(-\frac{1}{\beta}\left(\frac{X}{M^*}\right)^\beta\right) \qquad (45)$$

The expression for dt_N is shown in **Appendix IV**, together with the derivatives of some functions based on the t_{ij}-concept. Therefore, the plastic strain increment $d\varepsilon_{ij}^{p(IC)}$ is given by

$$d\varepsilon_{ij}^{p(IC)} = d\varepsilon_v^{p(IC)} \frac{\delta_{ij}}{3} = \frac{\frac{1}{t_{N1}}\langle dt_N \rangle}{\frac{1}{C_p}\left(1 + \frac{G(\rho)}{a_{kk}}\right)} \cdot \frac{\delta_{ij}}{3} \qquad (46)$$

where the symbol $\langle\rangle$ denotes the Macaulay bracket as mentioned before.

When the Cam clay model was formulated, it was based on Henkel's (1960) experimental results on normally consolidated clays, which showed a unique surface in p-q-e space independent of stress paths. Therefore, we assume that in the same way as the t_{ij}-clay model the present model satisfies the unique relation between ε_v^p and stresses at normally consolidated state ($\rho=0$; $G(\rho)=0$), even though the strain increment consists of the two components. From Eqs. (14), (21), (22) and (46), normally consolidated soils satisfy the following condition.

$$\frac{\partial f}{\partial \sigma_{kl}} d\sigma_{kl} = \frac{1}{C_p} d\varepsilon_v^p = \frac{1}{C_p} \left(d\varepsilon_v^{p(AF)} + d\varepsilon_v^{p(IC)}\right)$$

$$= \frac{1}{C_p}\left(\Lambda^{(AF)}\frac{\partial f}{\partial t_{ii}} + C_p \frac{1}{t_{N1}}\langle dt_N\rangle\right) \qquad (47)$$

From this equation, we can obtain the proportionality constant of $d\varepsilon_{ij}^{p(AF)}$ at normally consolidated state ($\rho=0$;

$G(\rho)=0$) by the following equation, which is the same as that in the t_{ij}-clay model (Nakai and Matsuoka, 1986).

$$\Lambda^{(AF)} = \frac{\frac{\partial f}{\partial\sigma_{kl}}d\sigma_{kl} - \frac{1}{t_{N1}}\langle dt_N\rangle}{\frac{1}{C_p}\frac{\partial f}{\partial t_{kk}}} = \frac{df_\sigma - \frac{1}{t_{N1}}\langle dt_N\rangle}{h^p} \qquad (48)$$

We then define the strain increment $d\varepsilon_{ij}^{p(AF)}$ at over-consolidated state as well as normally consolidated state in the following form, referring to Eqs. (33) and (48),

$$d\varepsilon_{ij}^{p(AF)} = \Lambda^{(AF)}\frac{\partial f}{\partial t_{ij}} = \frac{\frac{\partial f}{\partial\sigma_{kl}}d\sigma_{kl} - \frac{1}{t_{N1}}\langle dt_N\rangle}{\frac{1}{C_p}\left(\frac{\partial f}{\partial t_{mm}} + \frac{G(\rho)}{t_N}\right)} \cdot \frac{\partial f}{\partial t_{ij}}$$

$$= \frac{df_\sigma - \frac{1}{t_{N1}}\langle dt_N\rangle}{h^p} \cdot \frac{\partial f}{\partial t_{ij}} \qquad (49)$$

Hence, the strain increments, of which the stress path dependency on plastic flow is considered, are summarized as follows:

(i) elastic region ($\Lambda = df_\sigma/h^p < 0$):

$$d\varepsilon_{ij} = d\varepsilon_{ij}^e$$

$$= \frac{1+\nu_e}{E_e}d\sigma_{ij} - \frac{\nu_e}{E_e}d\sigma_{kk}\delta_{ij} \qquad (50)$$

(ii) elastoplastic region with strain hardening ($\Lambda = df_\sigma/h^p \geq 0$ and $h^p \geq 0$):

$$d\varepsilon_{ij} = d\varepsilon_{ij}^e + d\varepsilon_{ij}^{p(AF)} + d\varepsilon_{ij}^{p(IC)}$$

$$= \frac{1+\nu_e}{E_e}d\sigma_{ij} - \frac{\nu_e}{E_e}d\sigma_{kk}\delta_{ij}$$

$$+ \frac{\frac{\partial f}{\partial\sigma_{kl}}d\sigma_{kl} - \frac{1}{t_{N1}}\langle dt_N\rangle}{\frac{1}{C_p}\left(\frac{\partial f}{\partial t_{mm}} + \frac{G(\rho)}{t_N}\right)} \cdot \frac{\partial f}{\partial t_{ij}}$$

$$+ \frac{\frac{1}{t_{N1}}\langle dt_N\rangle}{\frac{1}{C_p}\left(1 + \frac{G(\rho)}{a_{kk}}\right)} \cdot \frac{\delta_{ij}}{3} \qquad (51)$$

(iii) elastoplastic region with strain softening ($\Lambda = df_\sigma/h^p \geq 0$ and $h^p < 0$):

$$d\varepsilon_{ij} = d\varepsilon_{ij}^e + d\varepsilon_{ij}^p$$

$$= \frac{1+\nu_e}{E_e}d\sigma_{ij} - \frac{\nu_e}{E_e}d\sigma_{kk}\delta_{ij}$$

$$+ \frac{\frac{\partial f}{\partial\sigma_{kl}}d\sigma_{kl}}{\frac{1}{C_p}\left(\frac{\partial f}{\partial t_{mm}} + \frac{G(\rho)}{t_N}\right)} \cdot \frac{\partial f}{\partial t_{ij}} \qquad (52)$$

Figure 12 shows the yield surface f and the present stress state A on the yield surface in t_N-t_S plane, in which the direction of plastic strain increment $d\varepsilon_{ij}^{p(AF)}$ is indicated by the arrow. Here, the directions of $d\varepsilon_{SMP}^{*p}$ and $d\gamma_{SMP}^{*p}$ coincide with those of t_N and t_S, respectively. When
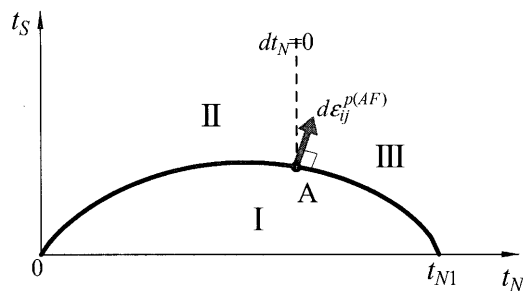
Fig. 12. Regions in which three kinds of strain increments occur

Table 2. Values of material parameters for Fujinomori clay

$C_f = \lambda/(1+e_0)$	5.08×10^{-2}	
$C_e = \kappa/(1+e_0)$	1.12×10^{-2}	
$N = e_{NC}$ at $p=98$kPa & $q=0$kPa	0.83	Same parameters as Cam clay model
$R_{CS} = (\sigma_1/\sigma_3)_{CS(comp.)}$	3.5	
ν_e	0.2	
β	1.5	Shape of yield surface (same as original Cam clay at $\beta=1$)
a	500	Influence of density and confining pressure

(a) stress ratio at peak R_f — density ρ relation

(b) stress ratio at peak R_f — initial OCR relation

Fig. 13. Calculated strength of Fujinomori clay

Fig. 14. Yield surface of Cam clay model and tension zone on p-q plane

Λ is negative and the stress state moves to inside the yield surface (region I), only elastic strain occurs. In the elastoplastic region with strain hardening where the stress state moves to region II, the plastic strain increment is only $d\varepsilon_{ij}^{p(AF)}$. On the other hand, if the stress state moves to region III, the plastic strain increment can be divided into $d\varepsilon_{ij}^{p(AF)}$ and $d\varepsilon_{ij}^{p(IC)}$. The present formulation allows continuous development of strain increment between region II and region III, and the directions of plastic flow are influenced by the stress path at region III. Now, though the proportionality constant $\Lambda^{(AF)}$ of $d\varepsilon_{ij}^{p(AF)}$ is negative if $df_\sigma - dt_N/t_{N1}$ becomes negative under some specific path in region III, it is confirmed numerically that the 2nd order plastic work increment $dt_{ij}d\varepsilon_{ij}^p$ is still positive even in such case, i.e., $dt_N(d\varepsilon_{SMP}^{*p(AF)} + d\varepsilon_{SMP}^{*p(IC)}) + dt_S(d\gamma_{SMP}^{*p(AF)} + d\gamma_{SMP}^{*p(IC)}) > 0$. The method to avoid the condition of $\Lambda^{(AF)} < 0$ in region III is also described in **Appendix V**.

FUNDAMENTAL FEATURE OF PRESENT MODEL AND VALIDATION BY TEST DATA ON CLAY

Material Parameters and Characteristics of Yield Surface

The present model is capable of describing deformation and strength behavior of not only clay but also sand. In this section, we will show the applicability of the model to clay just under triaxial compression and extension conditions. Table 2 shows the values of material parameters for saturated Fujinomori clay (F-clay), which is used for the validation of the model. Physical proper-
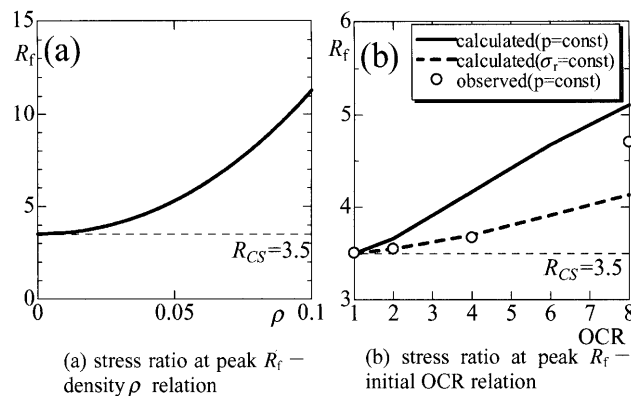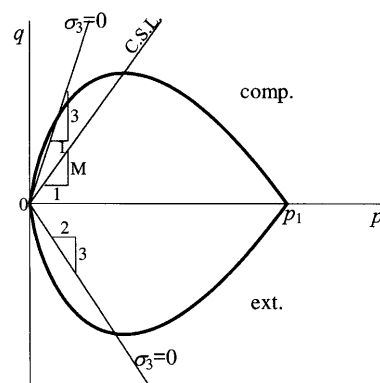
ties of the Fujinomori clay are as follows: the liquid limit $w_L = 44.7\%$, the plastic limit $w_P = 24.7\%$ and specific gravity $G_S = 2.65$. The methods of sample preparation are described in a previous paper (Nakai and Matsuoka, 1986). As indicated in the table, one parameter a is added to the parameters which are fundamentally the same as those of the Cam clay model. The values of parameters except for a can be determined from consolidation and shear tests on normally consolidated clay in the same way as the Cam clay model and t_{ij}-clay model (Nakai and Matsuoka, 1986). The value of a can be estimated from the strength of over-consolidated clay. The relation between stress ratio X_f at peak strength and density ρ is obtained from the condition of $h^p = 0$. This condition leads to

$$\frac{\partial f}{\partial t_{ii}} + \frac{a \cdot \rho^2}{t_N} = 0 \tag{53}$$

where

$$\frac{\partial f}{\partial t_{ii}} = \frac{1}{t_N}\left[a_{ii} + \frac{X^{\beta-2}}{M^{*\beta}}(x_{ii} - X^2 a_{ii})\right] \tag{54}$$

From this condition, we can obtain the relation between the peak strength $R_f = (\sigma_1/\sigma_3)_{f(comp)}$ and density ρ as in Fig. 13(a). Figure 13(b) shows the relation between peak strength and initial over-consolidation ratio on Fujinomori clay, which is also calculated by the present

model. As a method, we can estimate parameter a, utilizing this relation.

Figure 14 shows the yield surface of the Cam clay model for Fujinomori clay in p-q plane. Figure 15 shows the yield surface of the proposed model in (a) t_N-t_S plane and (b) p-q plane. In these figures, the upper half indicates the triaxial compression condition, and the lower half indicates the triaxial extension condition. We can see that the yield surface of t_{ij} model is symmetric with respect to the t_N-axis but not symmetric with respect to the p-axis. It is also noted that the direction of plastic flow of the t_{ij} model is not normal to the yield surface represented in the p-q plane, because the flow rule is assumed in modified stress t_{ij} space. Also, though the yield surface of the original Cam clay model is not

smooth at the tip on p-axis, that of the proposed model is smooth over the whole surface. The previous t_{ij} models for clay and sand also have singular points at the origin and the tip on the isotropic axis. Such smoothness of the present yield surface is one of the advantages in numerical computations in the same way as the modified Cam clay model (Roscoe and Burland, 1968). Now, the lines in which the minor principal stress σ_3 is zero are indicated in every figure. It can be seen that though models formulated using p and q such as the Cam clay model have tension zones on and inside the yield surface, there is no tension zone in the yield surface formulated using t_N and t_S. Models based on the t_{ij}-concept not only are capable of describing properly the influence of the intermediate principal stress but also have above-mentioned benefit for numerical computations.

Figure 16 shows the calculated relation between stress ratio $X \equiv t_S/t_N$ and plastic strain increment ratio $Y \equiv d\varepsilon^{*p}_{SMP}/d\gamma^{*p}_{SMP}$ for constant mean principal tests (solid curve) and constant stress ratio tests (symbols) on nor-

(a) Yield surface of proposed model and tension zone on $t_N - t_S$ plane

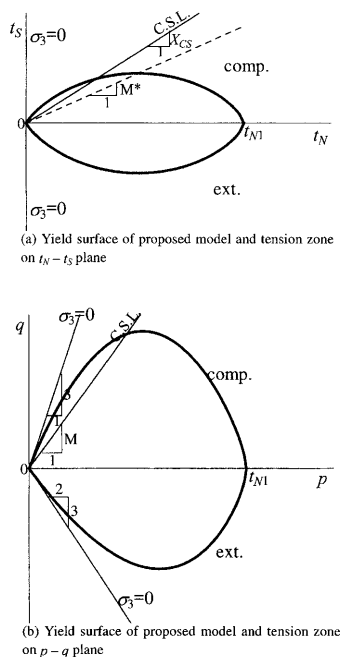(b) Yield surface of proposed model and tension zone on $p - q$ plane

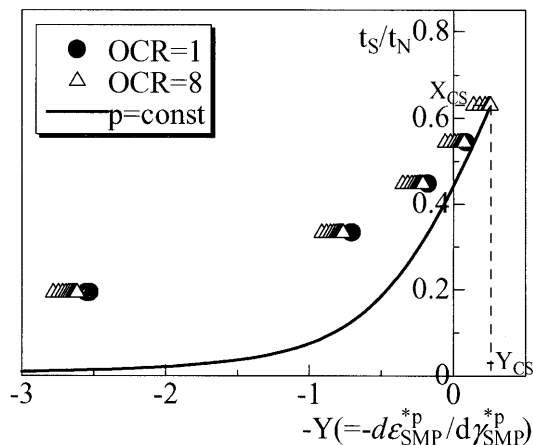**Fig. 15.   Yield surface of proposed model and tension zone**

Fig. 16.   Calculated relation between stress ratio and pastic strain increment ratio under constant stress ratio and under constant mean principal stress
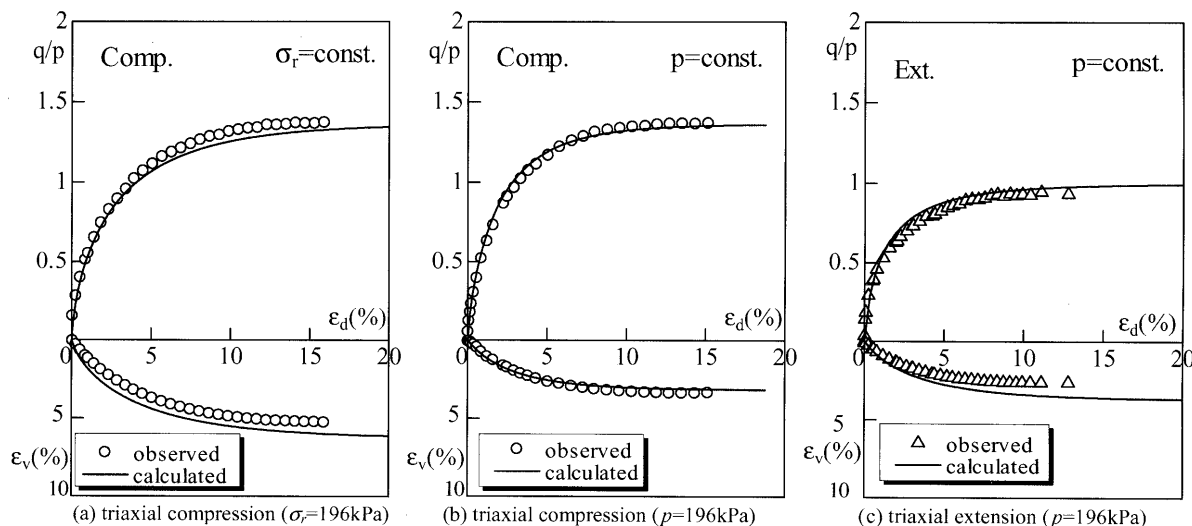

(a) triaxial compression (σ_r=196kPa)   (b) triaxial compression (p=196kPa)   (c) triaxial extension (p=196kPa)

Fig. 17.   Observed and calculated results of triaxial compression and extension tests on normally consolidated clay under monotonic loading
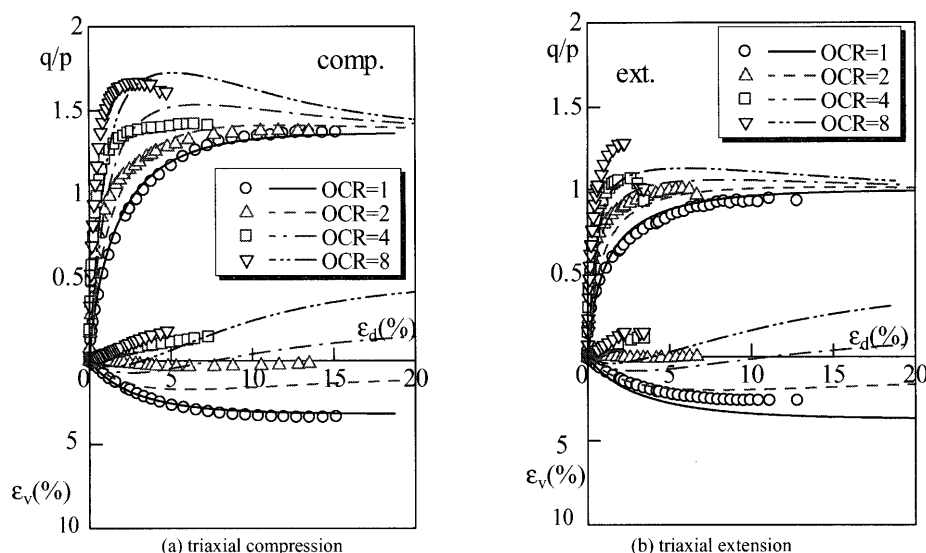
Fig. 18. Observed and calculated results of triaxial compression and extension tests with different over-consolidation ratio under monotonic loading
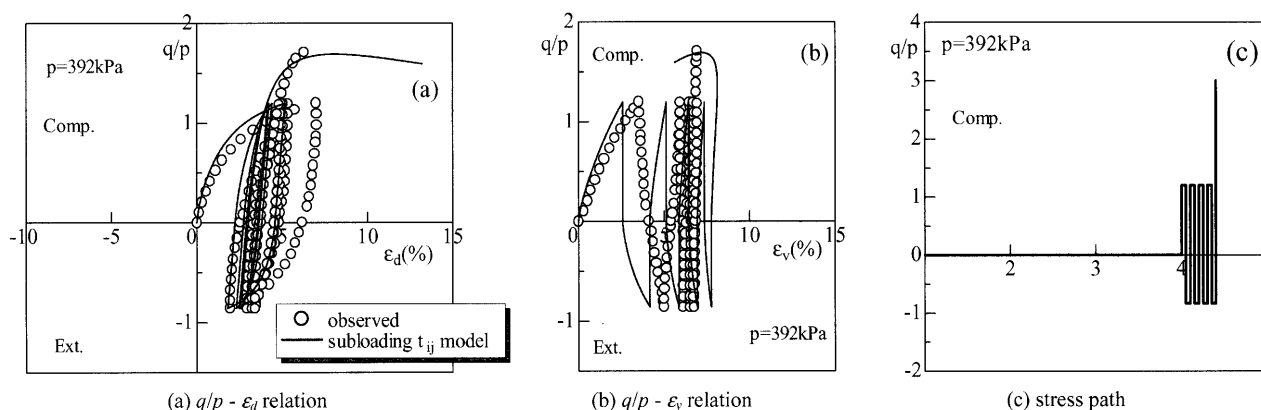

Fig. 19. Observed and calculated results of cyclic constant mean principal stress tests with constant amplitude of stress ratio

mally and over-consolidated clay. Here, the solid curve is the same as that in Fig. 7. It is known experimentally that the direction of plastic flow (plastic strain increment ratio) is influenced by the stress path before peak strength but is not influenced at peak strength. We can see from Fig. 16 that the present model can describe well such stress path dependency of plastic flow.

Triaxial Tests under Monotonic and Cyclic Loadings

Figure 17 shows the test results (dots) and the calculated curves of triaxial compression and extension tests on normally consolidated clay under monotonic loadings. Diagram (a) shows the results of the triaxial compression test under constant minor stress ($\sigma_3 = \sigma_r = 196$ kPa). Diagrams (b) and (c) are the results of triaxial compression and extension tests under constant mean principal tests ($p = 196$ kPa). We can see that the present model can describe well the deformation and strength of normally consolidated clay in triaxial compression and extension tests in the same way as the previous t_{ij}-clay model. Figure 18 shows the results of triaxial compression and extension tests on clays with different over-con-

solidation ratios (OCR = 1, 2, 4 and 8). Here, tests of OCR = 8 are carried out under $p = 98$ kPa, and the other tests are under $p = 196$ kPa. We can see from these figures that although the calculated curves for over-consolidated clays in triaxial extension still underpredict the strength and dilatancy, the model is capable of describing uniquely not only the influence of over-consolidation ratio on the deformation, dilatancy and strength of clay but also the influence of intermediate principal stress on them. Figures 19 to 21 are the results and stress paths of drained cyclic triaxial tests on normally consolidated clay. As shown the in stress path of diagram (c) in each figure, Fig. 19 is the cyclic constant mean principal test under constant amplitude of stress ratio, Fig. 20 is the results of the cyclic constant mean principal test under increasing stress ratio with number of cycles, and Fig. 21 is the results of cyclic constant radial stress test. We can see that in spite of using an isotropic hardening law, the proposed model can describe cyclic behavior of clay under triaxial conditions. This is due to the subloading surface concept and the loading condition in Eq. (35). The reason why the present model can describe the behavior of clays as they
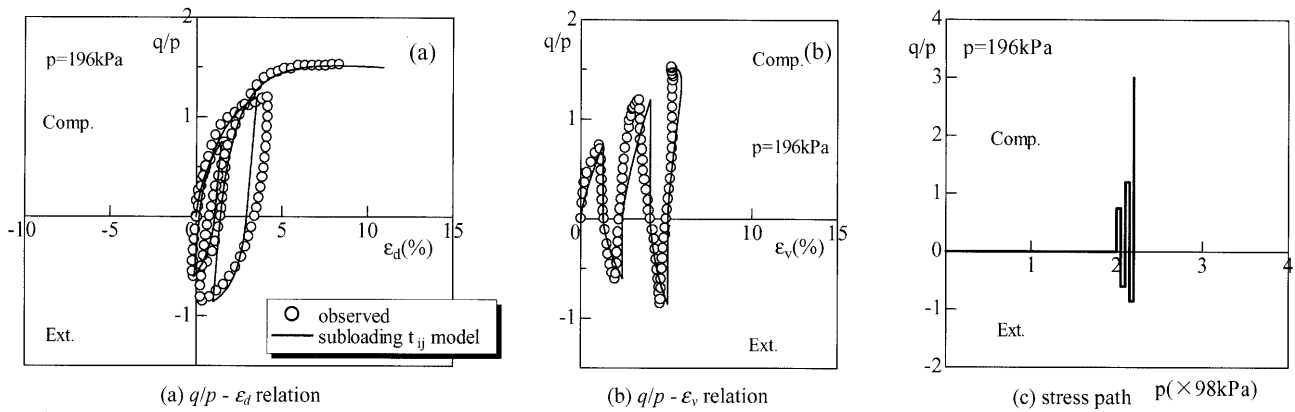
(a) q/p - ε_d relation   (b) q/p - ε_v relation   (c) stress path $p(\times 98\text{kPa})$

Fig. 20. Observed and calculated results of cyclic constant mean principal stress tests with increasing amplitude of stress ratio

(a) q/p - ε_d relation   (b) q/p - ε_v relation   (c) stress path $p(\times 98\text{kPa})$
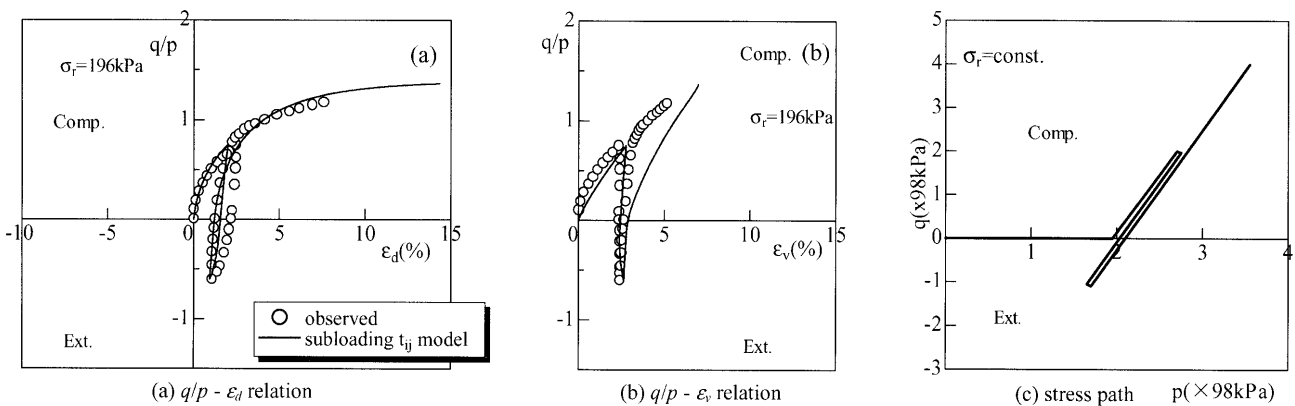
Fig. 21. Observed and calculated results of cyclic constant radial stress tests

become stiffer with increasing number of cycles is because the state variable ρ increases under cyclic loadings, even if the clay is initially normally consolidated ($\rho_0 = 0$). However, in the case of one-directional cyclic loading tests, the present model may overpredict the strains because of the isotropic subloading surface model.

VALIDATION BY TEST DATA ON SAND

Material Parameters and Triaxial Tests under Monotonic Loading

Toyoura sand (mean diameter $D_{50} = 0.2$ mm, uniformity coefficient $U_c = 1.3$, specific gravity $G_s = 2.65$, maximum void ratio $e_{max} = 0.95$, minimum void ratio $e_{min} = 0.58$) was used. Two kinds of procedures were used for preparing specimens of sand with different void ratios. Dense specimen was prepared by pouring the saturated sand into the mold in several layers and compacting each layer with a rod whose diameter was 6 mm so that the specimen had a desired void ratio ($e_{initial} \approx 0.68$). Loose specimen ($e_{initial} \approx 0.92$) was prepared by depositing the saturated sand slowly in de-aired water using a funnel with an opening of 3 mm. Both specimens, prepared in these ways, have quasi-isotropic structures. Every specimen was then consolidated isotropically to the prescribed stress state and then was sheared and/or consolidated

Table 3. Values of material parameters for Toyoura sand

λ	0.07	Same parameters as Cam clay model
κ	0.0045	
$N = e_{NC}$ at $p = 98\text{kPa}$ & $q = 0\text{kPa}$	1.1	
$R_{CS} = (\sigma_1/\sigma_3)_{CS(comp.)}$	3.2	
ν_e	0.2	
β	2.0	Shape of yield surface (same as original Cam clay at $\beta = 1$)
a a_{AF}	30	Influence of density and confining pressure
a_{IC}	500	

along the given stress paths.

Table 3 shows the values of material parameters for Toyoura sand. Unlike clay, the values of λ and N cannot be determined directly from isotropic consolidation test. This is because it is difficult to make the state of sand corresponding to the remolded normally consolidated clay. The dots in Fig. 22 are the observed results of isotropic compression tests on dense and loose sands, arranged in terms of the relation between void ratio e and

confining pressure p in logarithmic scale. So, assuming the normally consolidation line (NCL) as the broken line in this figure and referring to the relation between the density ρ, the peak strength X_f and the parameter a (*see* Eqs. (53) and (54)) of conventional triaxial compression tests in the same way as over-consolidated clay, we can draw the stress-strain curves to fit the observed ones. By
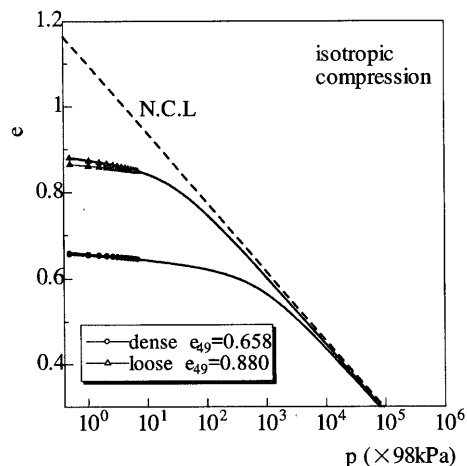
repeating this process by trial and error, a set of material parameters for sand is determined. Here, to get better fittings of the calculated curves to the data of shear tests and consolidation tests in Toyoura sand, different values of a ($a^{(AF)}$ and $a^{(IC)}$), which are the parameters of $G(\rho)$, are used for the two components ($d\varepsilon_{ij}^{p(AF)}$ and $d\varepsilon_{ij}^{p(IC)}$) in Eq. (51), respectively.

Figures 23 and 24 show the observed results (symbols) and the calculated curves of constant mean principal tests, constant major principal stress tests and constant minor principal stress tests on dense sand and loose sand, respectively. The plots in these figures are arranged in terms of the relation between stress ratio q/p, deviatoric strain ε_d and volumetric strain ε_v. In each figure, diagram (a) shows the results under triaxial compression condition, diagram (b) shows those under triaxial extension condition. We can see from these figures that the present model can describe the stress-strain-strength behavior, including the influence of stress paths, for sands under triaxial compression and extension conditions from dense state to loose state with unified material parameters.

The solid curves in Fig. 22 are the calculated e-log p relations in isotropic compression. The value of $a^{(IC)}$ in Table 3 is determined so that the curves to agree with the observed results represented by symbols. Figures 25 and

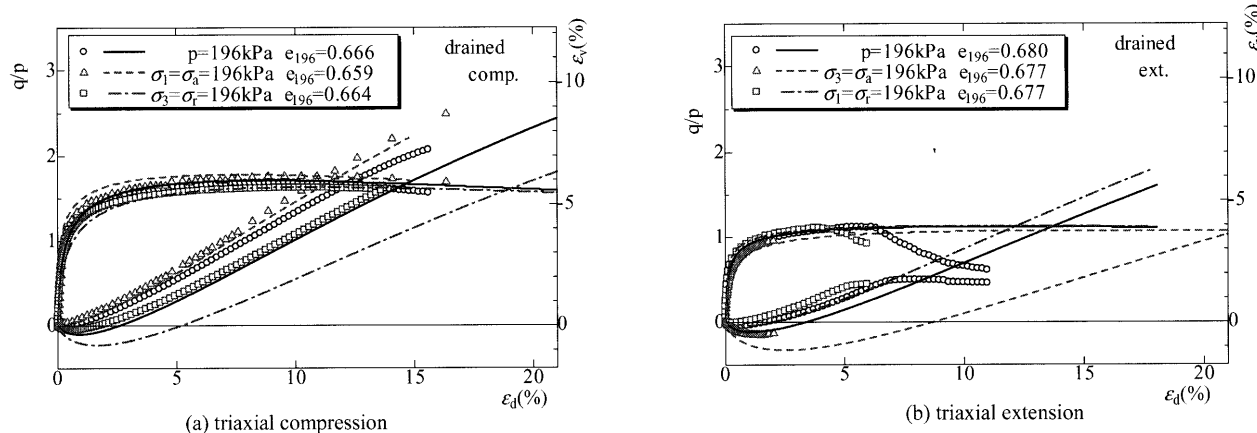Fig. 22.   Observed and calculated results of isotropic compression tests

Fig. 23.   Observed and calculated results of triaxial compression and extension tests on dense sand under monotonic loading
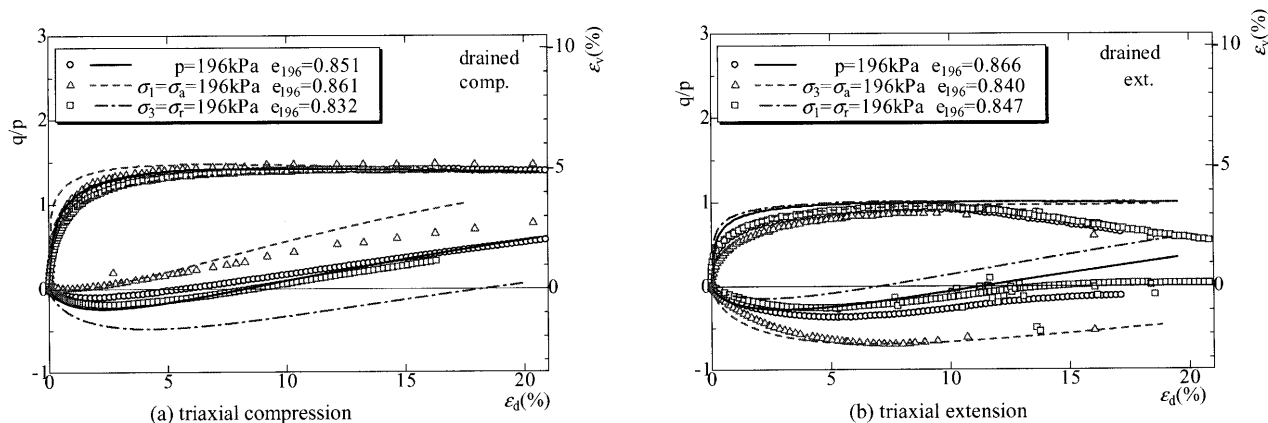

Fig. 24.   Observed and calculated results of triaxial compression and extension tests on loose sand under monotonic loading
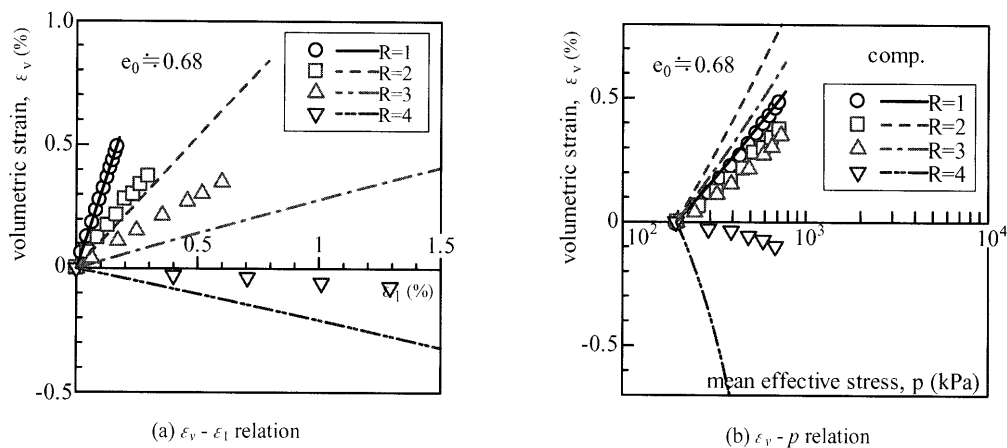
Fig. 25. Observed and calculated results of isotropic and anisotropic consolidation tests on dense sand under compression condition
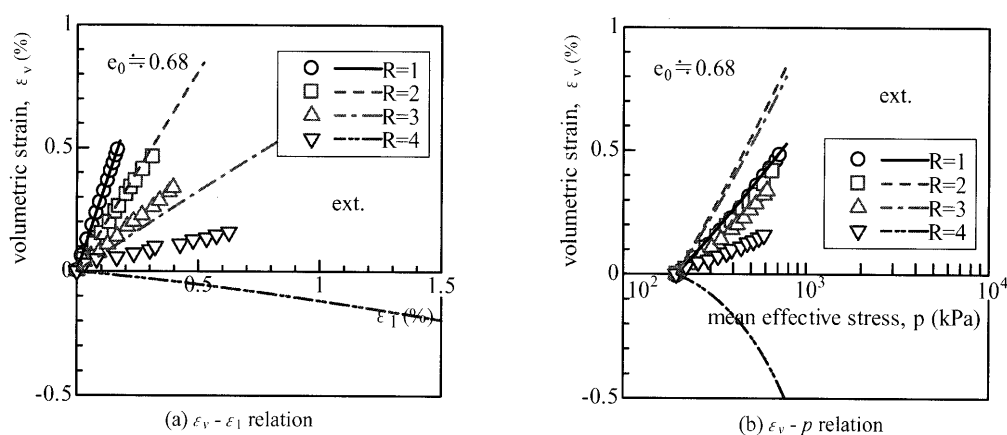

Fig. 26. Observed and calculated results of isotropic and anisotropic consolidation tests on dense sand under extension condition
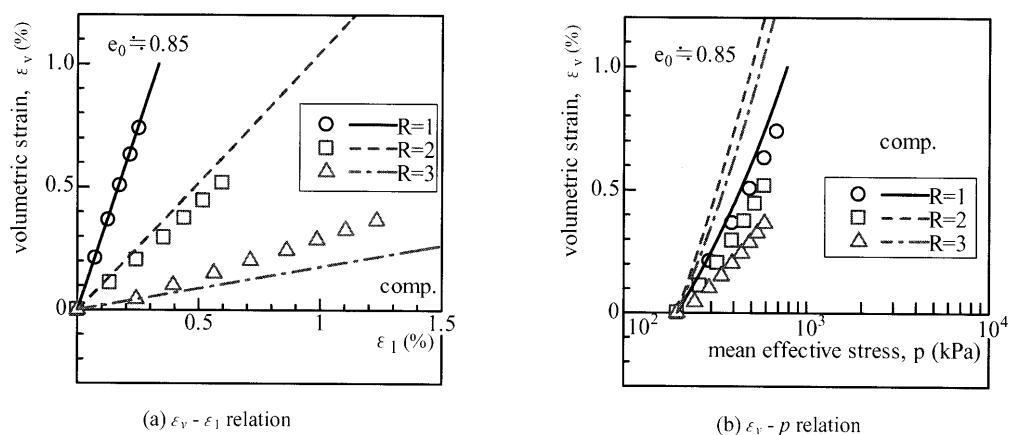

Fig. 27. Observed and calculated results of isotropic and anisotropic consolidation tests on loose sand under compression condition

26 show (a) the ε_v-ε_1 relation and (b) the ε_v-log p relation in isotropic and anisotropic consolidation tests on dense sand under triaxial compression and extension conditions, respectively. In these figures, R denotes the major-minor principal stress ratio σ_1/σ_3. The solid lines are the calculated results, and the symbols are the observed ones that are the same as those in the previous paper (Nakai, 1989). Figures 27 and 28 show the same arrangements on

loose sand. It can be seen from these figures that the model can describe the deformation behavior under anisotropic consolidation, though the model overestimates the positive dilatancy at large stress ratio ($R = 4$) in Figs. 25 and 26. If we employ the yield function (plastic potential function) derived from shear tests and do not consider the stress path dependency on the direction of plastic flow, the dilatancy under anisotropic consolida-
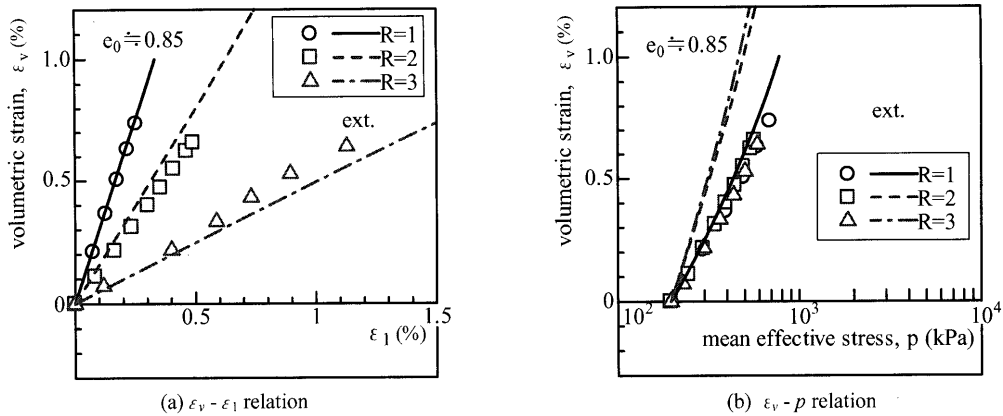
(a) ε_v - ε_1 relation

(b) ε_v - p relation

Fig. 28. Observed and calculated results of isotropic and anisotropic consolidation tests on loose sand under extension condition

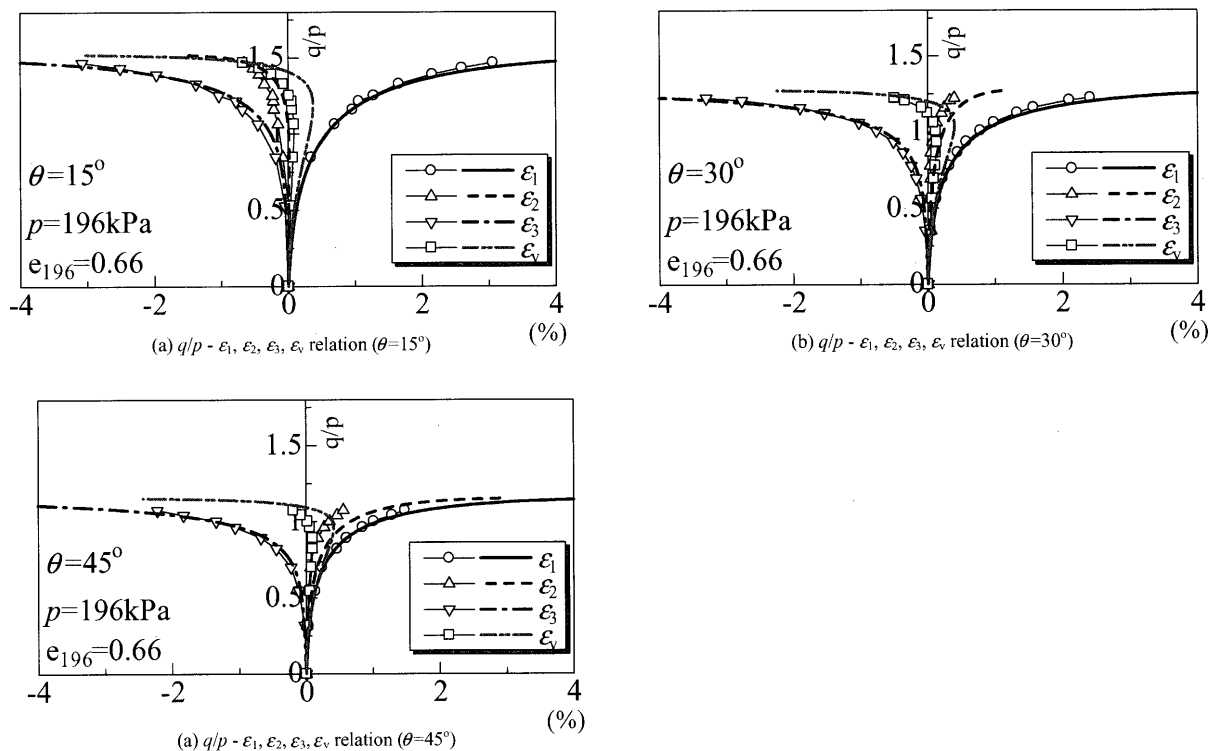(a) q/p - ε_1, ε_2, ε_3, ε_v relation ($\theta=15°$)

(b) q/p - ε_1, ε_2, ε_3, ε_v relation ($\theta=30°$)

(a) q/p - ε_1, ε_2, ε_3, ε_v relation ($\theta=45°$)

Fig. 29. Observed and calculated results of true triaxial tests on dense sand under monotonic loading

(a) Directions of calculated strain increments
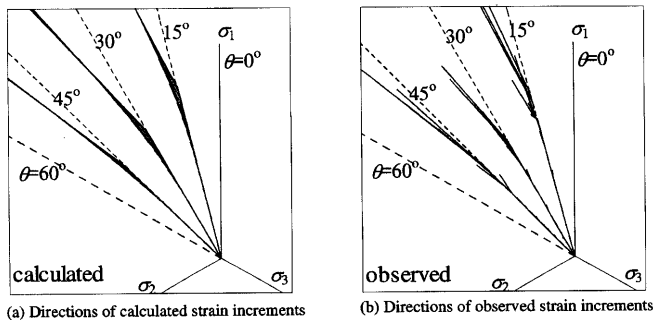
(b) Directions of observed strain increments

Fig. 30. Directions of observed and calculated strain increments on octahedral plane in true triaxial tests

tion is inevitably overestimated – e.g., overestimation of K_o value at one-dimensional consolidation.

True Triaxial Tests under Monotonic Loading

Using the experimental data on sand in the previous paper (Nakai, 1989), we will check the applicability of the present model in three different principal stresses. Figure 29 shows the observed (symbols) and calculated (curves) variations of the three principal strains (ε_1, ε_2 and ε_3) and the volumetric strain ε_v against stress ratio q/p in true triaxial tests ($\theta=15°$, 30° and 45°) on dense sand under constant mean principal stress ($p=196$ kPa). Figure 30 shows the observed and calculated directions of strain increments on the octahedral plane for these tests. Here, the length of each bar is proportional to the value

of shear strain increment divided by the shear-normal stress ratio increment on the octahedral plane. In each figure, θ denotes the angle between σ_1-axis and the corresponding radial stress path on the octahedral plane, where $\theta = 0°$ and $60°$ represent the stress path under triaxial compression and triaxial extension conditions, respectively. There is the following relation between the angle θ and the intermediate principal stress parameter b.

$$b = \frac{2 \tan \theta}{\sqrt{3} + \tan \theta} \qquad (55)$$

where b is represented using three principal stresses as

$$b = \frac{\sigma_2 - \sigma_3}{\sigma_1 - \sigma_3} \qquad (56)$$

As can be seen from Fig. 29, the present model predicts well the three-dimensional stress-strain behavior of sand in the same way as the previous model, though the previous one cannot consider the influence of the density and/or confining pressure. It is seen from Fig. 30 that the present model also predicts the observed tendency that the directions of strain increments deviate from the direction of shear stress with increase of stress ratio under three different principal stresses. From Figs. 29(a) and (b), i.e., ε_2 is negative in diagram (a) but is positive in diagram (b), we can presume that the stress condition θ in plane strain condition ($\varepsilon_2 = 0$) lies within $15° < \theta < 30°$, which is the same as results reported by many researchers.

CONCLUSIONS

The main results of this paper are summarized as follows:
(1)   A simple isotropic hardening elastoplastic model for soils (named subloading t_{ij} model) is formulated by extending previous models. As mentioned in the introduction; This model particularly considers some mechanical characteristics of soils, which the Cam clay model cannot describe,

○ (i)   Influence of intermediate principal stress on the deformation and strength of soil
○ (ii)   Stress path dependency of the direction of plastic flow
○ (iii)   Positive dilatancy during strain hardening
× (iv)   Soil anisotropy and non-coaxiality
◉ (v)   Behavior of soil under cyclic loading
○ (vi)   Influence of density and/or confining pressure on the deformation and strength
× (vii)   Behavior of structured soil
× (viii) Time effect and age effect

Here, marks ○, ◉ and × imply 'fully-considered', 'half-considered' and 'not-considered', respectively.
(2)   By referring to the subloading surface concept and test results on clays with different OCR, the previous t_{ij} clay model, which was applicable to normally consolidated clay, is extended to a model capable of describing the behavior of over-consolidated soils as well – i.e., the influence of density/or confining pressure. The present model also takes into consideration the influence of inter-

mediate principal stress using the t_{ij} concept.
(3)   This model is extended to one that can take into account the influence of stress path on the direction of plastic flow, without adding material parameter, by dividing the plastic strain increment into two components at the strain hardening region with increase of mean stress, in the same way as the previous t_{ij} clay model.
(4)   The present model can properly describe typical soil behavior of normally consolidated soil and over-consolidated soil in general stress conditions, though it has a few material parameters (fundamentally the parameters of Cam clay model plus one).
(5)   The validity of the model to clay is confirmed by conventional triaxial tests on normally consolidated clay and over-consolidated clays with different OCR under monotonic and cyclic loadings. It is also confirmed by conventional triaxial tests and true triaxial tests that the model can describe the deformation and strength behavior of sand with unified material parameters, regardless of soil density and confining pressure.

The present model has already been applied to the analyses of geotechnical problems such as bearing capacity problems (Nakai et al., 2001), localization problems (Hinokio et al., 2002), tunnel excavation problems (Shahin et al., 2004a and b) and so on in 2D and 3D conditions.

REFERENCES

1) Asaoka, A., Nakano, M. and Noda, T. (1994): Soil-water coupled behavior of saturated clay near/at critical state, *Soils and Foundations*, **34**(1), 91–106.
2) Asaoka, A., Nakano, M. and Noda, T. (1997): Soil-water coupled behavior of heavily overconsolidated clay near/at critical state, *Soils and Foundations*, **37**(1), 13–28.
3) Chowdhury, E. Q. and Nakai, T. (1998): Consequence of the t_{ij}-concept and a new modeling approach, *Computers and Geotechnics*, **23**, 131–164.
4) Chowdhury, E. Q., Nakai, T., Tawada, M. and Yamada, S. (1999): A model for clay using modified stress under various loading conditions with the application of subloading concept, *Soils and Foundations*, **39**(6), 103–116.
5) Hashiguchi, K. (1980): Constitutive equation of elastoplastic materials with elasto-plastic transition, *J. of Appli. Mech.*, ASME, **102**(2), 266–272.
6) Hashiguchi, K. and Ueno, M. (1977): Elasto-plastic constitutive laws for granular materials, constitutive equations for soils, *Proc. Specialty Session 9, 9th ICSMFE*, Tokyo, 73–82.
7) Henkel, D. J. (1960): The relationship between the effective stresses

and water content in saturated clays, *Geotechnique*, **10**, 44–54.

8) Hinokio, M., Nakai, T. and Aramaki, K. (2002): Numerical analysis using subloading t_{ij} model for localized deformation of clay based on small deformation theory, *Proc. 1st Int. Workshop on Frontiers in Computational Geotechnics*, Calgary, **1**, 75–82.

9) Matsuoka, H. and Nakai, T. (1974): Stress-deformation and strength characteristics of soil under three different principal stresses, *Proc. JSCE*, **232**, 59–70.

10) Nakai, T. (1989): An isotropic hardening elastoplastic model for sand considering the stress path dependency in three-dimensional stresses, *Soils and Foundations*, **29**(1), 119–137.

11) Nakai, T., Hinokio, M., Teranishi, T. and Hoshikawa, T. (2001): Load-settlement behavior of shallow foundation under various load conditions, *Proc. 15th ICSMGE*, Istanbul, **1**, 751–754.

12) Nakai, T. and Matsuoka, H. (1986): A generalized elastoplastic constitutive model for clay in three-dimensional stresses, *Soils and Foundations*, **26**(3), 81–98.

13) Nakai, T., Matsuoka, H., Okuno, N. and Tsuzuki, K. (1986): True triaxial tests on normally consolidated clay and analysis of the observed shear behavior using elastoplastic constitutive models, *Soils and Foundations*, **26**(4), 67–78.

14) Nakai, T. and Mihara, Y. (1984): A new mechanical quantity for soils and its application to elastoplastic constitutive models, *Soils and Foundations*, **24**(2), 82–94.

15) Roscoe, K. H. and Burland, J. B. (1968): On the generalized stress-strain behavior of wet clay, *Engineering Plasticity* eds. by Heyman and Leckie, F. A., Cambridge University Press, 535–609.

16) Schofield, A. N. and Wroth, C. P. (1968): *Critical State Soil Mechanics*, McGrow-Hill, London.

17) Shahin, H. M., Nakai, T., Hinokio, M., Kurimoto, T. and Sada, T. (2004): Influence of surface loads and construction sequence on ground response due to tunneling, *Soils and Foundations*, **44**(2), 71–84.

18) Shahin, H. M., Nakai, T., Hinokio, M. and Yamaguchi, D. (2004): 3D effects on pressure and displacements during tunnel excavations, *Soils and Foundations* (submitted).

APPENDIX I: CONCRETE EXPRESSION OF a_{ij}

The tensor a_{ij} is a dimensionless symmetric tensor whose principal axes coincide with those of stress σ_{ij}, so that it is obtained by transformation from its principal values $\hat{a}_{ij}$ as follows:

$$a_{ij} = Q_{im} Q_{jn} \hat{a}_{mn} \tag{A1}$$

Here, Q_{ij} is an orthogonal transformation that transforms ordinary stress (σ_{ij}) to their principal values ($\hat{\sigma}_{ij}$).

$$\hat{\sigma}_{ij} = Q_{mi} Q_{nj} \sigma_{mn} \tag{A2}$$

where

$$\hat{\sigma}_{ij} = \begin{pmatrix} \sigma_1 & 0 & 0 \\ 0 & \sigma_2 & 0 \\ 0 & 0 & \sigma_3 \end{pmatrix} \tag{A3}$$

and, from Eq. (2) $\hat{a}_{ij}$ is expressed as follows:

$$\begin{cases} \hat{a}_{ij} = \sqrt{\dfrac{I_3}{I_2 \hat{\sigma}_{ij}}} & \text{if } i = j \\ \hat{a}_{ij} = 0 & \text{if } i \neq j \end{cases} \tag{A4}$$

Particularly under plane strain and asymmetric conditions of ($\sigma_{33} = \hat{\sigma}_{33} = \sigma_3$ and $\sigma_{13} = \sigma_{23} = 0$), a_{ij} is expressed in the following manner. From Fig. A1, the angle 2α is given using σ_{ij} and $\hat{\sigma}_{ij}$ by
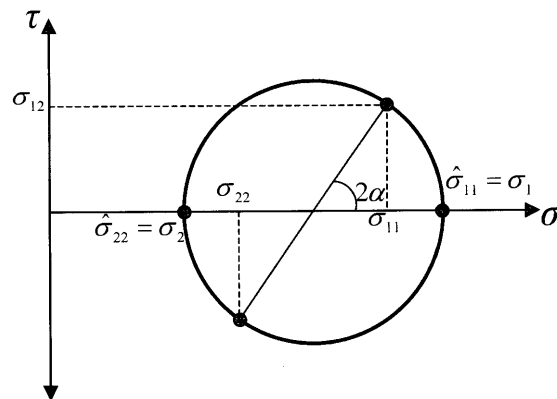

Fig. A1. Expression of σ_{ij} and $\hat{\sigma}_{ij}$ on Mohr's stress circle

$$\left. \begin{aligned} \cos 2\alpha &= \frac{\sigma_{11} - \sigma_{22}}{\sigma_1 - \sigma_2} = \frac{\sigma_{11} - \sigma_{22}}{\sqrt{(\sigma_{11} - \sigma_{22})^2 + 4\sigma_{12}^2}} \\ \sin 2\alpha &= \frac{2\sigma_{12}}{\sigma_1 - \sigma_2} = \frac{2\sigma_{12}}{\sqrt{(\sigma_{11} - \sigma_{22})^2 + 4\sigma_{12}^2}} \end{aligned} \right\} \tag{A5}$$

Therefore, a_{ij} is expressed as follows from the coaxiality between σ_{ij} and a_{ij}:

$$\left. \begin{aligned} a_{11} &= \frac{a_1 + a_2}{2} + \frac{a_1 - a_2}{2} \cos 2\alpha \\ a_{22} &= \frac{a_1 + a_2}{2} - \frac{a_1 - a_2}{2} \cos 2\alpha \\ a_{33} &= a_3 \\ a_{12} &= \frac{a_1 - a_2}{2} \sin 2\alpha \\ a_{23} &= a_{13} = 0 \end{aligned} \right\} \tag{A6}$$

APPENDIX II: DERIVATIONS OF M^*, X_{CS} AND Y_{CS}

Under triaxial compression condition, stress ratio $X \equiv t_S/t_N$ and strain increment ratio $Y \equiv d\varepsilon_{SMP}^{*p}/d\gamma_{SMP}^{*p}$ are expressed as follows (Nakai and Matsuoka, 1986):

$$X \equiv \frac{t_S}{t_N} = \frac{\sqrt{2}}{3}\left(\sqrt{\frac{\sigma_1}{\sigma_3}} - \sqrt{\frac{\sigma_3}{\sigma_1}}\right) \tag{A7}$$

$$Y \equiv \frac{d\varepsilon_{SMP}^{*p}}{d\gamma_{SMP}^{*p}} = \frac{d\varepsilon_1^p a_1 + 2d\varepsilon_3^p a_3}{\sqrt{2}(d\varepsilon_1^p a_3 + 2d\varepsilon_3^p a_1)}$$

$$= \frac{1 + 2\sqrt{\dfrac{\sigma_1}{\sigma_3}} \cdot \dfrac{d\sigma_3^p}{d\sigma_1^p}}{\sqrt{2}\left(\sqrt{\dfrac{\sigma_1}{\sigma_3}} + \dfrac{d\varepsilon_3^p}{d\varepsilon_1^p}\right)} \tag{A8}$$

Since $d\varepsilon_v^p = d\varepsilon_1^p + 2d\varepsilon_3^p = 0$ at critical state, stress ratio X_{CS} and plastic strain increment ratio Y_{CS} at critical state are expressed using the principal stress ratio at critical state $R_{CS} \equiv (\sigma_1/\sigma_3)_{CS(comp.)}$ as

$$X_{CS} = \frac{\sqrt{2}}{3}\left(\sqrt{R_{CS}} - \frac{1}{\sqrt{R_{CS}}}\right) \tag{A9; 17bis}$$

$$Y_{CS} = \frac{1 - \sqrt{R_{CS}}}{\sqrt{2}(\sqrt{R_{CS}} + 0.5)} \qquad \text{(A10; 18bis)}$$

Therefore, substituting $X = X_{CS}$ and $Y = Y_{CS}$ into Eq. (20), we can obtain the value of M^*, which represents the ordinate intercept of Eq. (20) in Fig. 7, as a function of R_{CS}

$$M^* = (X_{CS}{}^\beta + X_{CS}{}^{\beta-1} Y_{CS})^{1/\beta} \qquad \text{(A11; 16bis)}$$

APPENDIX III: PROPORTIONALITY CONSTANT Λ EXPRESSED BY STRAIN INCREMENT $d\varepsilon_{ij}$

Under elastoplastic region, the following equations hold:

$$d\sigma_{ij} = D^e_{ijkl} d\varepsilon^e_{kl} = D^e_{ijkl} (d\varepsilon_{kl} - d\varepsilon^p_{kl}) \qquad \text{(A12)}$$

$$d\varepsilon^p_{ij} = \Lambda \frac{\partial f}{\partial t_{ij}} \qquad \text{(A13; 21bis)}$$

$$\Lambda = \frac{\dfrac{\partial f}{\partial \sigma_{ij}} d\sigma_{ij}}{h^p} \qquad \text{(A14; 33bis)}$$

From Eqs. (A12) and (A14), we can obtain

$$\Lambda \cdot h^p = \frac{\partial f}{\partial \sigma_{ij}} d\sigma_{ij} = \frac{\partial f}{\partial \sigma_{ij}} D^e_{ijkl} (d\varepsilon_{kl} - d\varepsilon^p_{kl}) \qquad \text{(A15)}$$

Substituting Eq. (A13) into Eq. (A15) leads

$$\Lambda = \frac{\dfrac{\partial f}{\partial \sigma_{ij}} D^e_{ijkl} d\varepsilon_{kl}}{h^p + \dfrac{\partial f}{\partial \sigma_{mn}} D^e_{mnop} \dfrac{\partial f}{\partial t_{op}}} \qquad \text{(A16)}$$

APPENDIX IV: PARTIAL DERIVATIVES OF YIELD FUNCTION AND STRESS VARIABLES

Generally, the yield function of the isotropic hardening model based on t_{ij}-concept is given by the following form as a function of mean stress t_N and stress ratio X

$$f = f(t_N, X) = \ln t_N + \varsigma(X) - \ln t_{N1} = 0 \qquad \text{(A17)}$$

and definitions of tensors and scalars related to t_{ij}-concept are shown in Table 1.

We will first show the derivatives of f with respect to modified stress t_{ij}.

$$\frac{\partial f}{\partial t_{ij}} = \frac{\partial f}{\partial t_N} \frac{\partial t_N}{\partial t_{ij}} + \frac{\partial f}{\partial X} \frac{\partial X}{\partial t_{ij}} \qquad \text{(A18)}$$

$$\frac{\partial f}{\partial t_N} = \frac{1}{t_N} \qquad \text{(A19)}$$

$$\frac{\partial t_N}{\partial t_{ij}} = \frac{\partial (t_{kl} a_{kl})}{\partial t_{ij}} = a_{ij} \qquad \text{(A20)}$$

$$\frac{\partial f}{\partial X} = \varsigma'(X) \qquad \text{(A21)}$$
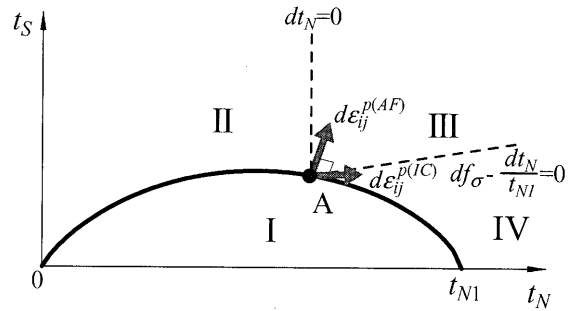

Fig. A2. Regions in which four kinds of strain increments occur

$$\frac{\partial X}{\partial t_{ij}} = \frac{\partial(\sqrt{x_{kl} x_{kl}})}{\partial x_{mn}} \frac{\partial x_{mn}}{\partial t_{ij}} = \frac{1}{X \cdot t_N} (x_{ij} - X^2 a_{ij}) \qquad \text{(A22)}$$

Next, the derivative of f with respect to the ordinary stress σ_{ij} is expressed as follows:

$$\frac{\partial f}{\partial \sigma_{ij}} = \frac{\partial f}{\partial t_N} \frac{\partial t_N}{\partial \sigma_{ij}} + \frac{\partial f}{\partial X} \frac{\partial X}{\partial \sigma_{ij}} \qquad \text{(A23)}$$

$$\frac{\partial t_N}{\partial \sigma_{ij}} = \frac{\partial}{\partial \sigma_{ij}} \left(3 \frac{I_3}{I_2} \right) \qquad \text{(A24)}$$

$$\frac{\partial X}{\partial \sigma_{ij}} = \frac{\partial}{\partial \sigma_{ij}} \left(\sqrt{\frac{I_1 I_2}{9 I_3}} - 1 \right) \qquad \text{(A25)}$$

where, I_1, I_2 and I_3 are the first, second and third invariants of σ_{ij} as shown in Eq. (3). Therefore, the terms df_σ and dt_N can be given using general stress increment $d\sigma_{ij}$.

APPENDIX V: METHOD TO AVOID $\Lambda^{(AF)} < 0$ IN STRAIN HARDENING REGION

The value of $\Lambda^{(AF)}$ becomes negative in the region IV in Fig. A2. It is then assumed that the total plastic strain increment occurs isotropically such as

$$d\varepsilon^p_{ij} = \Lambda^{(IC)} \frac{\delta_{ij}}{3} \qquad \text{(A26)}$$

Referring to Eq. (46) and considering the compatibility condition and the smooth change of the plastic strain development at the boundary between region III and IV, lead to the following equation

$$df = \frac{\partial f}{\partial \sigma_{ij}} d\sigma_{ij} - \frac{1}{C_p} \left(d\varepsilon^p_v - d\left(\frac{\rho}{1+e_0} \right) \right)$$

$$= \frac{\partial f}{\partial \sigma_{ij}} d\sigma_{ij} - \frac{1}{C_p} \left(\Lambda^{(IC)} + \Lambda^{(IC)} \frac{G(\rho)}{a_{kk}} \right) = 0 \qquad \text{(A27)}$$

Therefore, $\Lambda^{(IC)}$ in Eq. (A26) is given by

$$\Lambda^{(IC)} = \frac{\dfrac{\partial f}{\partial \sigma_{ij}} d\sigma_{ij}}{\dfrac{1}{C_p} \left(1 + \dfrac{G(\rho)}{a_{kk}} \right)} \qquad \text{(A28)}$$